Significance of *BRCA2* and *RB1* Co-loss in Aggressive Prostate Cancer Progression

Goutam Chakraborty[1], Joshua Armenia[2], Ying Z. Mazzu[1], Subhiksha Nandakumar[2], Konrad H. Stopsack[1], Mohammad O. Atiq[1], Kazumasa Komura[1,3], Lina Jehane[1], Rahim Hirani[1], Kalyani Chadalavada[4], Yuki Yoshikawa[1], Nabeela A. Khan[1], Yu Chen[1,5], Wassim Abida[1], Lorelei A. Mucci[6], Gwo-Shu Mary Lee[7], Gouri J. Nanjangud[4], and Philip W. Kantoff[1]

ABSTRACT

Purpose: Previous sequencing studies revealed that alterations of genes associated with DNA damage response (DDR) are enriched in men with metastatic castration-resistant prostate cancer (mCRPC). *BRCA2*, a DDR and cancer susceptibility gene, is frequently deleted (homozygous and heterozygous) in men with aggressive prostate cancer. Here we show that patients with prostate cancer who have lost a copy of *BRCA2* frequently lose a copy of tumor suppressor gene *RB1*; importantly, for the first time, we demonstrate that co-loss of both genes in early prostate cancer is sufficient to induce a distinct biology that is likely associated with worse prognosis.

Experimental Design: We prospectively investigated underlying molecular mechanisms and genomic consequences of co-loss of *BRCA2* and *RB1* in prostate cancer. We used CRISPR-Cas9 and RNAi-based methods to eliminate these two genes in prostate cancer cell lines and subjected them to *in vitro* studies and transcriptomic analyses. We developed a 3-color FISH assay to detect genomic deletions of *BRCA2* and *RB1* in prostate cancer cells and patient-derived mCRPC organoids.

Results: In human prostate cancer cell lines (LNCaP and LAPC4), loss of *BRCA2* leads to the castration-resistant phenotype. Co-loss of *BRCA2-RB1* in human prostate cancer cells induces an epithelial-to-mesenchymal transition, which is associated with invasiveness and a more aggressive disease phenotype. Importantly, PARP inhibitors attenuate cell growth in human mCRPC-derived organoids and human CRPC cells harboring single-copy loss of both genes.

Conclusions: Our findings suggest that early identification of this aggressive form of prostate cancer offers potential for improved outcomes with early introduction of PARP inhibitor–based therapy.

See related commentary by Mandigo and Knudsen, p. 1784

Introduction

Pathologic variants of DNA damage response (DDR) genes are prevalent in a subset of men with metastatic castration-resistant prostate cancer (mCRPC; refs. 1–3). DDR is an essential defense and cell survival mechanism (4). Inherited (germline) or somatic genetic abnormalities of DDR pathway components, primarily insertions or deleterious mutations resulting in protein truncations, occur in 20%–25% of men with mCRPC (1–3). Although *BRCA2* mutations are known to confer an increased risk of breast and ovarian cancer (5), recent observations have shown that alterations of *BRCA2* are more prevalent than previously appreciated in men with prostate cancer and more frequent than alterations in any other DDR gene (6). In one study, *BRCA2* alterations were seen in 13.3% of men with metastatic prostate cancer, while another found germline *BRCA2* mutations in 5.3% of men with advanced prostate cancer (2, 3). Importantly, in a cohort of 1,302 men with localized and locally advanced prostate cancer, the 67 patients with *BRCA2* germline mutations experienced more rapid progression to mCRPC, with 5-year metastasis-free survival rates of approximately 50%–60%, suggesting a more aggressive phenotype (7). A very recent germline sequencing study in a large cohort of men (7,636 unselected patients with prostate cancer and 12,366 male, cancer-free controls) revealed that pathologic variants of *BRCA2* were significantly associated with prostate cancer risk ($P < 0.001$; ref. 8). Deep sequencing of cell-free DNA (cfDNA) from 202 patients with mCRPC treated with abiraterone acetate or enzalutamide after development of CRPC revealed that defects in *BRCA2* and *ATM* were strongly associated with poor clinical outcomes and resistance to these second-generation antiandrogens, independent of other prognostic factors (9). The mechanisms by which loss of *BRCA2* might promote aggressive prostate cancer and confer resistance to androgen deprivation therapy (ADT) and androgen signaling pathway inhibitors are not understood.

Previous studies have shown that loss of *RB1* is associated with CRPC progression and metastasis (10, 11). Earlier studies showed that disruption of *RB1* modulates androgen receptor (AR) activity in prostate cancer that in turn induces castration resistance and resistance to AR-directed therapeutics, and that the tumor-suppressive function of *RB1* is distinct from canonical cell-cycle regulation of *RB1* (12, 13). Very recently, Abida and colleagues showed that *RB1* alteration was significantly associated with poor overall survival for 128 patients with mCRPC treated with first-line next-generation AR signaling inhibitors (ARSi; abiraterone or enzalutamide; $P = 0.002$;

[1]Department of Medicine, Memorial Sloan Kettering Cancer Center, New York, New York. [2]Center for Molecular Oncology, Memorial Sloan Kettering Cancer Center, New York, New York. [3]Department of Urology, Osaka Medical College, Osaka, Japan. [4]Molecular Cytogenetics Core Facility, Memorial Sloan Kettering Cancer Center, New York, New York. [5]Human Oncology Pathogenesis Program, Memorial Sloan Kettering Cancer Center, New York, New York. [6]Department of Epidemiology, Harvard T.H. Chan School of Public Health, Boston, Massachusetts. [7]Department of Medicine, Dana-Farber Cancer Institute, Boston, Massachusetts.

Note: Supplementary data for this article are available at Clinical Cancer Research Online (http://clincancerres.aacrjournals.org/).

Current address for J. Armenia: IMED Biotech Unit, AstraZeneca, Cambridge, United Kingdom.

Corresponding Author: Philip W. Kantoff, Memorial Sloan Kettering Cancer Center, 1275 York Avenue, New York, NY 10065. Phone: 212-639-5851; Fax: 929-321-5023; E-mail: kantoff@mskcc.org

Clin Cancer Res 2020;26:2047–64

doi: 10.1158/1078-0432.CCR-19-1570

©2019 American Association for Cancer Research.

Downloaded from http://aacrjournals.org/clincancerres/article-pdf/26/8/2047/2067287/2047.pdf by guest on 27 August 2022

Translational Relevance

Mechanisms underlying the relationship between DNA damage response (DDR) defects and prostate cancer progression are poorly understood. Although germline and somatic mutations of the DDR gene *BRCA2* are increased in metastatic castration-resistant prostate cancer (mCRPC) compared with primary localized prostate cancer, the role of *BRCA2* alteration in primary localized prostate cancer is not well characterized. We discovered that even single copy loss of *BRCA2* and its chromosomal neighbor *RB1* in primary tumors is sufficient to induce an aggressive form of early prostate cancer and may be associated with a poor prognosis. Using cell lines and patient-derived organoids, we also demonstrate that co-loss of *BRCA2* and *RB1* likely enhances sensitivity of prostate cancer cells to PARP inhibitors, offering a potential treatment strategy for this aggressive form of early prostate cancer.

ref. 14). *RB1* is located on chromosome 13q in close proximity to *BRCA2*. Deletion of chromosome 13q is a frequent event in localized prostate cancer and related to clinical aggressiveness (15, 16). Deletion (loss of heterozygosity) of 13q was associated with higher prostate cancer stage and grade and is common in metastatic disease (17). Moreover, in a study of 7,375 prostate cancer cases, 21% of localized cases harbored deletion of 13q; this deletion was associated with advanced tumor stage and early biochemical recurrence (18). Another prostate cancer study demonstrated that *BRCA2* germline mutations are often associated with *RB1* heterozygous deletion (19).

Herein, we identify a previously uncharacterized prostate cancer subset characterized by concomitant deletions (homozygous and heterozygous) of *BRCA2* and *RB1*. Furthermore, for the first time, we demonstrate that even single copy loss of *BRCA2* and *RB1* is sufficient to induce an aggressive phenotype in prostate cancer. In this study, we developed a cell line–based model to examine the consequence of codeletion of *BRCA2* and *RB1* and demonstrated that this alteration is an independent genomic driver of therapy-resistant aggressive prostate cancer rather than the consequence of exposure to therapy. We further show that co-loss of *BRCA2* and *RB1* may induce an epithelial-to-mesenchymal transition (EMT) mediated by induction of the transcription factors SLUG or SNAIL or transcriptional coactivator PRRX1.

Tumors that harbor DDR defects, particularly *BRCA* defects, are sensitive to PARP inhibitors (PARPi) through a synthetic lethality mechanism (20). In a phase II clinical trial of olaparib in 49 patients with mCRPC, 16 (∼33%) showed a significant response to therapy (radiologic progression–free survival $P < 0.001$, overall survival $P = 0.05$). Of note, 88% of responders to olaparib harbored homologous recombination repair defects, due, in large part, to aberrations of *BRCA2* and *ATM* (1). In our study, we developed a 3-color FISH method for rapid identification of codeletion of *BRCA2* and *RB1* in human prostate cancer cells and in mCRPC organoids. We show that PARP inhibition significantly attenuates growth of prostate cancer cell lines and organoids derived from human mCRPC that harbor not only homozygous but also heterozygous codeletion of *BRCA2* and *RB1*. We propose that early recognition and intervention using PARPi-based therapy in prostate cancer cases identified as having *BRCA2-RB1* codeletion could lead to substantial clinical benefit.

Materials and Methods

Cell culture

Human prostate cancer cells LNCaP, 22RV1, DU145, PC3, and VCaP were obtained from ATCC. LNCaP-C42 cells were obtained from VitroMed. The LNCaP-Abl cell line was provided by Zoran Culig (Innsbruck Medical University, Innsbruck, Austria), E006AA-T cells were provided by John T. Isaacs (The Johns Hopkins University School of Medicine, Baltimore, MD), PC3M cells were provided by Raymond C. Bergan (Knight Cancer Institute, Oregon Health & Science University, Portland, OR), and the LAPC4 cell line was provided by Charles Sawyers (Memorial Sloan Kettering Cancer Center, New York, NY). These cells were maintained in 10% FBS (LNCaP, LNCaP-C42, LAPC4, VCaP, 22RV1, DU145, PC3, PC3M, and E006AA) or 10% charcoal-stripped serum (LNCaP-Abl) supplemented with 2 mmol/L of L-glutamine and 1× antibiotic/antimycotic (Gemini Bio-Products) at 37°C in 5% CO_2. Human prostate epithelial cell RWPE1 was obtained from ATCC and cultured in keratinocyte serum-free medium (Thermo Fisher Scientific) at 37°C in 5% CO_2. Cells were authenticated by human short tandem repeat profiling at the MSK Integrated Genomics Operation Core. Patient-derived human prostate cancer organoids were cultured as described previously (21).

CRISPR, gene expression, and gene silencing

Lentiviral vectors encoding CRISPR or short hairpin RNA (shRNA) were generated as described previously (22) and transfected to LNCaP cells using LentiBlast (OZ Biosciences). Stable cells were generated using puromycin and/or hygromycin selection. We have designed three separate guide RNAs (gRNA) for human *BRCA2* and human *RB1* (Supplementary Table S1) and cloned the gRNAs into a Lenti-CRISPRv2-puromycin or hygromycin backbone respectively; a third-generation lentiviral backbone that constitutively expresses Cas9. Nontargeting scrambled gRNA (scr gRNA) was used as control. We used a similar strategy for generating 22RV1-*RB1* cells and LNCaP-*RB1* cells.

To generate *BRCA2* knockout LNCaP cells by CRISPR/CAS9 methods, we infected parental LNCaP cells with *BRCA2* scr gRNA lentivirus, followed by 5 μg/mL puromycin for 5 days. Loss of *BRCA2* in the pooled population of LNCaP cells was analyzed by Western blot analysis using *BRCA2*-specific antibodies and this pooled population of cells was used for the following experiments. For generation of single cell–derived clones, we plated *BRCA2* pooled population cells in very low density (500 cells in each 150-mm tissue culture plate in 20 mL of puromycin-supplemented media). After 4 weeks, single cell–derived clones were isolated using PYREX cloning cylinders (Thermo Fisher Scientific # 99-552-21). To determine the genome targeting efficiency of *BRCA2* scr gRNA in the pooled population as well as in single cell–derived clones, we performed T7 endonuclease assay using EnGen Mutation detection kit according to manufacturer's protocol (NEB). The primers corresponding to specific gRNA that were used for PCR amplification are listed in Supplementary Table S1. The T7 assay demonstrated a mixed heterozygous population of cells containing wild-type (wt) and mutant *BRCA2* DNA (Supplementary Fig. S1B).

To generate *BRCA2* knockout RWPE1 cells, we cloned *BRCA2* gRNA2 to LentiCRISPRv2-GFP backbone that constitutively expresses Cas9 and GFP. Lentiviral infected cells were selected by FACS sorting for GFP-positive cells (twice) and analyzed by Western blot analysis. To generate BRCA2-RB1 knockout–knockdown *LNCaP* cells, we first infected parental LNCaP cells with lentivirus containing *BRCA2* gRNA or scr gRNA. Pooled populations of the stable cells were established by puromycin selection and analyzed by Western blot

Downloaded from http://aacrjournals.org/clincancerres/article-pdf/26/8/2047/2067287/2047.pdf by guest on 27 August 2022

analysis and qPCR. We infected BRCA2-knockout or scr LNCaP cells with lentivirus containing *RB1* shRNA followed by hygromycin selection. BRCA2-knockout or scr (gRNA) LNCaP cells also infected with lentiviral nontargeting shRNA (scr-shRNA) were used as control. Cells within 4–10 passages after stable selection were used for the following experiments.

siRNA or cDNA constructs were transiently transfected to indicated cells using the TransIT-X2 system (Mirus). A list of CRISPR, cDNA, shRNA, and SMARTpool siRNA constructs is provided in Supplementary Table S1. Efficiency of knockdown and overexpression was verified by qPCR and Western blot analysis.

Bioinformatic analysis of clinical cohorts

Bioinformatic analysis of publicly available genomics data from various clinical cohorts was performed using data obtained from cBioPortal (23, 24) and Oncomine (25). The graphs and Kaplan–Meier survival curves were plotted using GraphPad Prism (version 7). Also used in this study were the cohorts described in the following sources: Armenia and colleagues 2018 (26); Baca and colleagues 2013 (27); Barbieri and colleagues 2012 (28); Beltran and colleagues 2016 (29); Grasso and colleagues 2012 (30); Hieronymus and colleagues 2014 (31); Kumar and colleagues 2016 (32); Robinson and colleagues 2015 (3); Setlur and colleagues 2008 (33); Taylor and colleagues 2010 (34); TCGA 2015 (35); TCGA provisional and pan-cancer prostate, TCGA provisional pan-cancer (unpublished data in cBioPortal); and Zehir and colleagues 2017 (36).

Western blot analysis

Cells were washed with HBSS and lysed in radioimmunoprecipitation assay (RIPA) buffer unless otherwise noted (50 mmol/L TRIS-HCl pH 7.4, 150 mmol/L NaCl, 1 mmol/L EDTA, 1% Triton X-100, 1% sodium deoxycholate, and 0.1% SDS) supplemented with protease and phosphatase inhibitors (Thermo Fisher Scientific). Protein concentrations were measured using the Bradford protein assay. Western blot was performed using specific antibodies (Supplementary Table S1). For *BRCA2* Western blot we used Novex Tris-Glycine Mini Gels, WedgeWell format (6% or 4%–20%, Thermo Fisher Scientific).

RNA extraction and qPCR

Total RNA was extracted using the Direct-zol RNA Kit (Zymo Research) and reverse transcribed with qScript cDNA SuperMix (Quantabio). cDNA corresponding to approximately 10 ng of starting RNA was used for one reaction. qPCR was performed with Taqman Gene Expression Assay (Applied Biosystems). All quantifications were normalized to endogenous GAPDH. Probes used for qPCR are listed in Supplementary Table S1.

RNA-sequencing and pathway analyses

Total RNA from indicated cells and control LNCaP cells were isolated and analyzed by RNA sequencing by 50 million 2 × 50 bp reads in the MSK Integrated Genomics Operation Core Facility. RNA-sequencing data were analyzed in Partek. Heatmaps and volcano plots were developed using Partek manufacturer's instructions. Pathway analysis from RNA-sequencing data was performed using gene set enrichment analysis (GSEA) and ToppGene (37). The Molecular Signatures Database (MSigDB) is currently the most useful tool to analyze gene set enrichment from the transcriptomic data (38). Liberzon and colleagues developed a collection of "hallmark" gene sets as a part of MSigDB that summarize and represent specific well-defined biological states or processes and display coherent expression (39). These "hallmark pathways" summarize information across multiple gene sets and therefore provide more defined biological space for GSEA analysis (39). We used this hallmark signature to analyze our RNA sequencing and clinical cohort transcriptome data. Sequencing data are deposited to GEO repository under accession number GSE114155.

For the generation of survival curves using 10-gene (upregulated or downregulated from RNA sequencing) signatures, the Z score for each gene in 10-gene signatures was generated on the basis of the mRNA expression data from the Taylor cohort by using only the subset of primary prostate cancer samples. mRNA signature score was obtained by summing the Z scores. This generated a unique value for each sample in the cohort; this score was then divided into low and high based on the median. These mRNA scores were then correlated to clinical outcomes in the Taylor cohort. The Kaplan–Meier survival curves were generated and compared using the log-rank test.

3D Matrigel organoid assays

3D organoid assays were performed as described previously (40). Cells were detached using Accutase (Innovative Cell Technologies), collected using 70-μm cell strainers, counted (1×10^3 cell/well), and resuspended in serum-free PrEGM BulletKit (Lonza, catalog no. CC-3165 and CC-4177) supplemented with 1:50 B-27 supplement (Thermo Fisher Scientific catalog no. 17504044) and mixed with Matrigel Membrane Matrix (Thermo Fisher Scientific CB-40234C) in a 1:1 ratio. The cell and Matrigel mixture were plated on ultra-low attachment plates and allowed to grow for 2 weeks in serum-free PrEGM BulletKit supplemented with 1:50 B-27 medium. Organoids were counted and photographed using GelCount colony counter (Oxford Optronix). Organoid diameters more than 100 μm were counted.

Immunofluorescence study

Cells were plated on cover slips and allowed to grow for 48 hours. Cells were washed with HBSS and fixed in 4% paraformaldehyde for 10 minutes. Cells were permeabilized in 0.2% Triton X100 for 20 minutes in room temperature and blocked in blocking solution (2.5% BSA, 2.5% goat, and 2.5% donkey serum in HBSS) for 1 hour at room temperature followed by incubation with indicated primary antibody in blocking solution in 4°C overnight and then secondary antibody for 1 hour at room temperature. For Phalloidin staining, fixed cells were incubated in 1× Alexa Fluor 594 Phalloidin (Thermo Fisher Scientific) at 4°C overnight. Cells were mounted in mounting media containing DAPI and visualized and photographed under a fluorescent microscope (Nikon).

Cell proliferation assay by MTT, BrdU, and crystal violet

For MTT assay, cells were plated at 2.5×10^3 per well in 96-well plates in complete media (10% FBS) or media supplemented with 10% charcoal-stripped serum. Cells were either treated with DMSO or with indicated inhibitors. After indicated times, cells were incubated in 0.5 mg/mL MTT (Invitrogen) for 1 hour at 37°C. MTT crystals were dissolved in isopropanol and absorbance was measured in BioTek plate reader at 570 nm and represented graphically. The BrdU assay was performed by BrdU Cell Proliferation Assay Kit according to manufacturer's instructions (BrdU cell proliferation assay kit, Cell Signalling Technology, # 6813). Cells were plated at 2.5×10^3 per well in 96-well plates in complete media (10% FBS) or media supplemented with 10% charcoal-stripped serum. Cells were either treated with DMSO or with indicated inhibitors. BrdU incorporation in the proliferating cells was

Downloaded from http://aacrjournals.org/clincancerres/article-pdf/26/8/2047/2067287/2047.pdf by guest on 27 August 2022

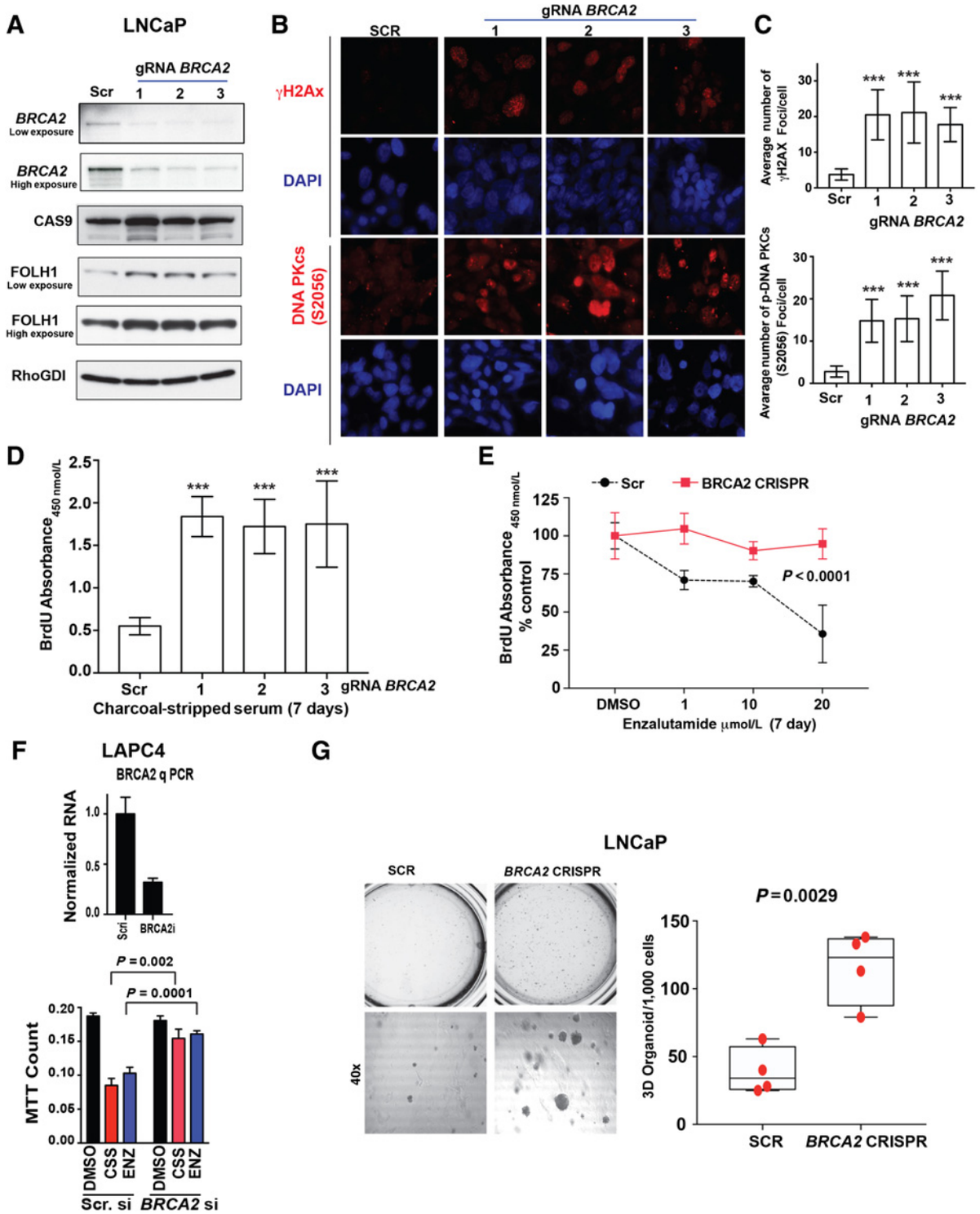

Figure 1.

BRCA2 loss induces castration resistance in prostate cancer cells. **A,** Western blot showing protein in LNCaP cells transduces three different guide RNAs (gRNA) targeting *BRCA2* (CRISPR-*BRCA2*). Cells infected with scrambled (scr) gRNA were used as control. Cas9 and RHoGDI served as loading controls. **B,** Immunofluorescence study of phospho-γ-H2Ax (pγH2AX) and DNA-PKcs (S2056) in *BRCA2* CRISPR-edited LNCaP cells. Nuclei were stained with DAPI (blue). **C,** The bar graphs show pγH2AX and DNA-PKcs (S2056) positive foci counted in high power field. *P* values determined by Student *t* test. ***, $P < 0.001$. **D** and **E,** Bar graph and growth curve showed the proliferation of LNCaP *BRCA2* CRISPR-edited and nontargeting control gRNA (scr) infected cells in charcoal-stripped medium (CSS) or complete medium supplemented with enzalutamide (ENZ; indicated concentration) for 7 days. (*Continued on the following page.*)

Downloaded from http://aacrjournals.org/clincancerres/article-pdf/26/8/2047/2067287/2047.pdf by guest on 27 August 2022

measured in BioTek plate reader at 450 nm and represented graphically. For the Crystal Violet cell proliferation assay, cells (in 96-well plate, treated with indicated drugs or cultured in FBS or CSS supplemented medium) were fixed in chilled 100% methanol for 10 minutes followed by staining with crystal violet (Millipore Sigma) for 2 hours and then washed with water. Crystal violet was dissolved in 1% SDS and absorbance was measured in BioTek plate reader at 595 nm and represented graphically.

Wound scratch assay

Control and indicated LNCaP or RWPE1 cells were seeded at a density of 0.5×10^5 cells per 24-well cell culture plate in complete medium. After 48 hours, a scratch was made with a 10 μL pipette tip in a confluent area of the cell culture dish. Photographs of a selected area of each scratch were taken 48 hours after scratching.

Matrigel invasion and Boyden chamber migration assay

Matrigel invasion and Boyden chamber migration assays were performed as described previously (41). Briefly, cells in serum-free media (2.5×10^3 cells/well for control LNCaP and variants; 1×10^3 for PC3M and variants) were added in the top of the Matrigel invasion chamber (Thermo Fisher Scientific catalog no. 08-774-122) or Corning migration chamber (Thermo Fisher Scientific catalog no. 07-200-174). Ten percent FBS in the bottom chamber was used as chemoattractant. After indicated times, cells in the bottom chamber were fixed in methanol and stained with crystal violet, photographed, and counted under phase-contrast microscopy.

FISH analysis

All cell lines were harvested and fixed in methanol: acetic acid (3:1). FISH analysis was performed on fixed cells and was based on TCGA data (Supplementary Fig. S3D; ref. 35). A 3-color probe was designed to detect loss of *BRCA2* (red) and *RB1* (orange). Region 13q12 (green) served as the control. The bacterial artificial chromosome (BAC) clones used in the probe-mix were as follows: *BRCA2* (RP11-281G19; labeled with red dUTP), RB1 (RP11-305D15; labeled with orange dUTP), and 13q12 (RP11-867N8 and RP11-1031D16; labeled with green dUTP). All RP11 clones were purchased from the Roswell Park Cancer Institute Genomics Shared Resource (Buffalo, NY). Probe labeling, hybridization, posthybridization washing, and fluorescence detection were performed according to standard laboratory procedures. Prior to hybridization on cell lines, the probe was hybridized on normal peripheral blood (male) and locus specificity was confirmed. Slides were scanned using a Zeiss Axioplan 2i epifluorescence microscope (Carl Zeiss Microscopy) equipped with a 1.4-megapixel CCD camera (CV-M4+CL, JAI) controlled by Isis 5.5.9 imaging software (MetaSystems Group Inc).

The entire hybridized area was scanned through a 63× or 100× objective lens to assess quality of hybridization and signal pattern. Following initial scan, for each cell line, a minimum of 100 nuclei were scored and representative cells/regions imaged. A minimum of 25 metaphases were also analyzed and chromosomes counted to infer ploidy. The call for loss was in relation to ploidy; for example, in a near-tetraploid (∼4n) cell line, copy number ≤3 was considered as loss. Three normal lymphoblastoid cell lines (GM06875A, GM07535B, and GM21677), obtained from Corielle Institute (Camden, NJ), were also analyzed and for each cell line, a minimum of 100 nuclei scored to derive the cut-off values (false-positive). The cut-off value for each gene/locus was calculated as the mean of false-positive plus three times the SD and set at 5% for loss (<2 copies) and applicable to diploid cell lines.

Statistical analysis

Results are reported as mean ± SD or ± SEM, unless otherwise noted. Comparisons between groups were performed using an unpaired two-sided Student *t* test ($P < 0.05$ was considered significant), unless noted. *P* trends were analyzed by one-way ANOVA. Bar graphs were generated using GraphPad Prism software (version 7.0 GraphPad Software, Inc).

Results

Elimination of *BRCA2* leads to therapy resistance in prostate cancer cell lines

We investigated the consequences of *BRCA2* deletion via lentiviral CRISPR/Cas9-mediated stable elimination of *BRCA2* in LNCaP cells, a hormone-dependent human prostate cancer cell line. All three gRNAs successfully diminished *BRCA2* transcript and protein levels in LNCaP cells (**Fig. 1A**; Supplementary Fig. S1A top and bottom). Furthermore, the T7 endonuclease assay revealed that all three gRNAs induced heterozygous loss of *BRCA2* in LNCaP cells (Supplementary Fig. S1B). Previous studies demonstrated that *BRCA2* inactivation impairs homologous recombination of DNA double-strand breaks and therefore *BRCA2*-null cells become sensitive to PARPi (42). As predicted, *BRCA2*-null LNCaP cells exhibited enhanced sensitivity to various PARPi and cisplatin (Supplementary Fig. S1C). However, our data also showed that *BRCA2* knockout LNCaP cells exhibited more sensitivity toward talazoparib (BMN 673) and rucaparib compared with control gRNA (scr) infected cells (Supplementary Fig. S1C). We detected higher expression of *FOLH1* in *BRCA2* knockout LNCaP cells compared with control cells (**Fig. 1A**). We observed that elimination of *BRCA2* increases phosphorylation of γH2AX in LNCaP cells (**Fig. 1B** and C, top), a biomarker for defective repair of double-strand breaks, indicating that CRISPR-mediated elimination of *BRCA2* may induce a homologous recombination repair defect in LNCaP cells. We also observed an increase in S2056 autophosphorylation of DNA-PKcs in *BRCA2* knockout LNCaP cells, indicating hyperactivation of DNA-PKcs (**Fig. 1B** and C, bottom). Furthermore, *BRCA2*-null LNCaP cells exhibited androgen-independent growth, as evidenced by enhanced 2D growth in androgen-deprived charcoal-stripped medium compared with control LNCaP (**Fig. 1D**, Supplementary Fig. S1E and S1F). Also, the *BRCA2*-null LNCaP cells exhibited relative resistance to

(*Continued.*) Equivalent volume of DMSO was used as placebo treatment. Cell growth was measured by BrdU incorporation assay (see Materials and Methods; ±SD); *P* values determined by Student *t* test. ***, $P < 0.001$. **F,** Parental LAPC4 cells were transiently transfected with *BRCA2*-specific SMARTpool siRNA for 96 hours. Total RNA was isolated, and *BRCA2* mRNA was analyzed by qPCR. Scrambled SMARTpool siRNA–transfected cells were used as control (top). *BRCA2*- or scrambled SMARTpool siRNA-transfected LAPC4 cells were cultured in charcoal-stripped medium (CSS) or complete medium supplemented with enzalutamide (ENZ; 20 μmol/L) for 72 hours after transfection (bottom). Equivalent volume of DMSO was used as placebo treatment. Cell growth was measured by MTT assay; SD, *P* values determined by Student *t* test. **G,** Control and CRISPR-edited LNCaP cells (10^3 cells/well) were mixed with Matrigel, and 3D cell cultures (organoids) were grown for 7 days in androgen-depleted, growth factor–enriched media. The photographs show the picture of the 24-well plate at day 7 (top left) and the 40× magnification images of representative 3D organoids (bottom left). Graph (right) shows the number of 3D organoids (>100 μm diameter, ± SD); each point represents the number of organoids grown from 10^3 cells in each individual well, *P* value determined by Student *t* test.

Downloaded from http://aacrjournals.org/clincancerres/article-pdf/26/8/2047/2067287/2047.pdf by guest on 27 August 2022

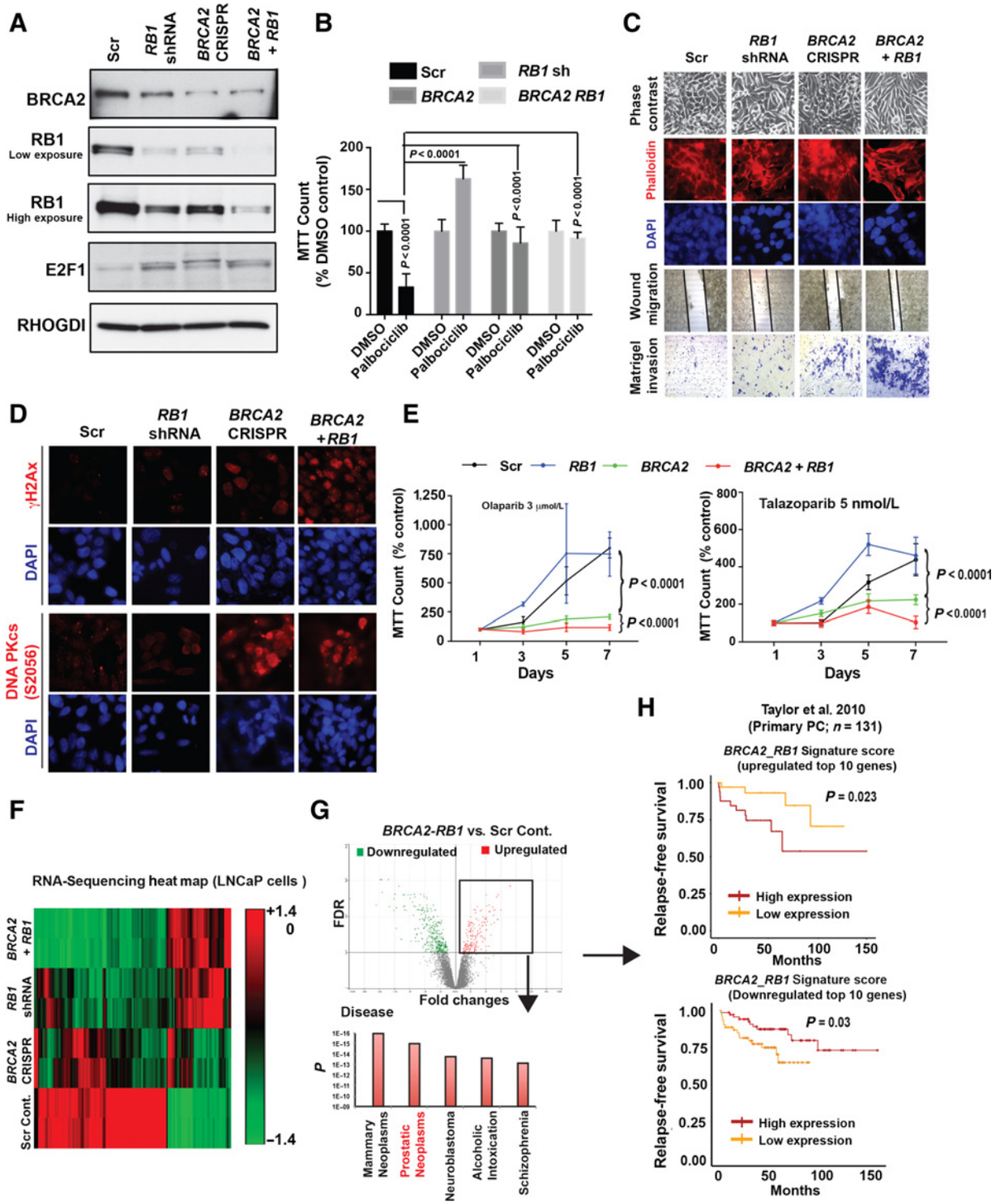

Figure 2.

Co-loss of *BRCA2* and *RB1* induces invasive phenotype in LNCaP cells. **A,** Western blot showing indicated protein levels in LNCaP-*BRCA2* CRISPR-edited (CRISPR gRNA 2) and nontargeting gRNA–infected control (Scr-CRISPR) cells infected with lentiviral *RB1* short hairpin RNA (shRNA). Scr-CRISPR and *BRCA2*-CRISPR2 cells also transfected with nontargeting shRNA (scr-Sh) for control of shRNA. RHoGDI served as the loading control. **B,** Indicated cells were treated with 3 μmol/L palbociclib (CDK4/6 inhibitor) for 3 days. Equivalent volume of DMSO was used as placebo treatment. Cell growth was measured by MTT assay; SD, *P* values determined by Student *t* test. **C,** Top row, phase contrast bright-field micrograph (200× magnification) showing the morphology of LNCaP cells after infection with indicated CRISPR/shRNA in stable lentiviral vector. Second and third rows: Immunofluorescence (400× magnification) of f-actin filament stained with phalloidin in indicated CRISPR/shRNA–infected LNCaP cells. Nuclei were stained with DAPI (blue). Note that LNCaP-*BRCA2-RB1* cells exhibit cytoskeleton rearrangement compared with scrambled control LNCaP cells. (*Continued on the following page.*)

Downloaded from http://aacrjournals.org/clincancerres/article-pdf/26/8/2047/2067287/2047.pdf by guest on 27 August 2022

enzalutamide (**Fig. 1E**; Supplementary Fig. S1D and S1F), indicating that these cells became castration resistant. Similarly, RNAi-mediated transient silencing of *BRCA2* in LNCaP and LAPC4 (another androgen-dependent human prostate cancer cell line) cells also exhibited resistance to androgen depletion, as evidenced by growth in charcoal-stripped medium or complete media supplemented with enzalutamide (Supplementary Fig. S1G; **Fig. 1F**) *BRCA2*-null LNCaP cells also exhibited enhanced prostatosphere formation in 3D Matrigel cultures (organoids) in the androgen-independent condition (**Fig. 1G**) indicating that *BRCA2*-null LNCaP cells are more tumorigenic compared with control LNCaP cells.

Concomitant elimination of *BRCA2* and *RB1* induces an invasive phenotype in human prostate cancer cells

To investigate the direct effect of the *BRCA2-RB1* codeletion on human prostate cancer cells, we introduced a shRNA of *RB1* (shRB1; in a lentiviral stable expression vector) into *BRCA2*-null LNCaP cells, generating *BRCA2-RB1* knockdown LNCaP cells (hereafter called LNCaP-*BRCA2-RB1*; **Fig. 2A**; Supplementary Fig. S2A). We observed downregulation of *BRCA2* protein and mRNA in *RB1* knockdown LNCaP cells (**Fig. 2A**; Supplementary Fig. S2A). Interestingly, we have also observed that loss of *BRCA2* attenuates RB1 protein expression in all *BRCA2* knockout LNCaP cells (**Fig. 2A**; Supplementary Fig. S2B). Similarly, CRISPR-mediated knockout of *RB1* also inhibits *BRCA2* expression in LNCaP cells (Supplementary Fig. S2C), indicating a possible feed-forward loop between *BRCA2* and *RB1* expression in prostate cancer cells. We observed induction of E2F-1 in *RB1* and/or *BRCA2* knockdown/knockout cells (**Fig. 2A**). Furthermore, *BRCA2-RB1* knockout/knockdown LNCaP cells exhibit relative resistance to the CDK4/6 inhibitor palbociclib as determined by MTT assay (**Fig. 2B**). Our data suggest that depletion of *RB1* and/or *BRCA2* in LNCaP cells is sufficient to induce canonical downstream pathway suppression by *RB1*.

LNCaP-*BRCA2-RB1* cells exhibited elongated morphology (**Fig. 2C**). Immunofluorescence staining using phalloidin shows the remodeling of actin filaments in LNCaP-*BRCA2-RB1* cells, further supporting the changes of cellular morphology upon co-loss of *BRCA2* and *RB1* (**Fig. 2C**). LNCaP-*BRCA2-RB1* cells also exhibited enhanced wound migration and invasion through Matrigel (**Fig. 2C**; Supplementary Fig. S2D). Knockdown/knockout of either *RB1* or *BRCA2* alone induced an intermediate invasive phenotype (**Fig. 2C**; Supplementary Fig. S2D).

We observed increased phosphorylation of γH2AX in LNCaP-*BRCA2-RB1* cells compared with *BRCA2* or *RB1* knockout/knockdown LNCaP cells (**Fig. 2D**; Supplementary Fig. S2E). Furthermore, we observed a very modest increase of S2056 autophosphorylation of DNA-PKcs in LNCaP-*BRCA2-RB1* cells compared with *BRCA2* knockout LNCaP cells (**Fig. 2D**; Supplementary Fig. S2F). *RB1* loss alone only caused a modest increase of phosphorylation of γH2AX but not S2056 autophosphorylation of DNA-PKcs compared with control LNCaP cells (**Fig. 2D**; Supplementary Fig. S2F). Treatment with the PARPi olaparib and talazoparib caused more cell growth inhibition in LNCaP-*BRCA2-RB1* cells than on *BRCA2*-null LNCaP cells (**Fig. 2E**). We were unable to detect any inhibitory effect of olaparib or talazoparib on *RB1* knockdown cells compared with control LNCaP cells. These data suggested that co-loss of *BRCA2* and *RB1* increases sensitivity to PARPi in prostate cancer cells compared with *BRCA2* loss alone. In contrast, *RB1* loss alone was not associated with sensitivity of prostate cancer cells to PARPi (**Fig. 2E**).

To further confirm the effect of co-loss of *BRCA2* and *RB1* on the invasive phenotype of prostate cancer cells, we knocked out *RB1* in 22RV1 cells that harbor oncogenic mutation of *BRCA2* (T3033Nfs*11; **Fig. 5B**). *RB1* knockout 22RV1 cells exhibit higher Matrigel invasion compared with control 22RV1 cells (Supplementary Fig. S2G).

To understand the molecular consequence of *BRCA2-RB1* loss, we performed RNA sequencing on the LNCaP-*BRCA2-RB1* cells. Interestingly, we observed a gradation of changes in gene expression in these cells compared with knockdown of either *BRCA2* or *RB1* alone, which provided further evidence of an additive effect of *BRCA2-RB1* co-loss in LNCaP cells (**Fig. 2F**; Supplementary Table S2). Pathway analysis of upregulated genes in LNCaP-*BRCA2-RB1* cells showed that the gene signature is prostate cancer–specific (**Fig. 2G**, top and bottom; Supplementary Table S3). Using single-sample GSEA (ssGSEA; ref. 43), we developed a 10-gene signature from the 10 mRNAs most upregulated and most downregulated (Supplementary Table S2) by co-loss of *BRCA2* and *RB1* in LNCaP cells. Both 10-gene signatures strongly predicted early relapse in localized prostate cancer in the Taylor cohort (**Fig. 2H**). In addition, we performed GSEA on the upregulated transcriptome of LNCaP-*BRCA2-RB1* cells (Supplementary Fig. S2H; Supplementary Table S3) and observed that induction of several essential molecular pathways, including regulation of cell differentiation and transcription, were enriched upon co-loss of *BRCA2* and *RB1* in LNCaP cells. However, we are unable to detect any correlation between previously published *RB1* signatures (12, 44) and our LNCaP cell–derived *BRCA2-RB1* signature (Supplementary Figs. S2I and S2J).

Coelimination of *BRCA2* and *RB1* leads to EMT

Our observations prompted us to investigate the molecular mechanism by which the invasive phenotype resulting from co-loss of *BRCA2* and *RB1* in LNCaP cells occurs. We performed the "hallmark pathways" analysis using GSEA in the upregulated transcriptome of LNCaP-*BRCA2-RB1* cells (**Fig. 2G**, top). We observed increased expression of several EMT and dedifferentiation-related signaling pathways (mTORC1, Hedgehog, TNFα-NFκB, TFGβ), including

(*Continued.*) Fourth row: micrographs (in 40× magnification) of 24-hour wound migration of indicated cells (see Materials and Methods). Bottom row, 5×10^3 indicated cells were plated on the top of Boyden chamber (see Materials and Methods) in serum-free media; 10% serum in the bottom chamber was used as chemoattractant. After 48 hours, cells in the bottom side of the chamber were fixed, stained, and photographed (100× magnification). **D,** Immunofluorescence images showing phospho-gamma H2x (pγH2AX) and DNA-PKcs (S2056) in indicated LNCaP cells. Nuclei were stained with DAPI (blue). **E,** Indicated cells were treated with PARP inhibitors (olaparib 3 μmol/L, talazoparib 0.005 μmol/L) for indicated days. The graphs show cell growth measured by MTT assay (±SD); *P* values determined by Student *t* test. **F,** RNA sequencing followed by hierarchical clustering of the genes altered in LNCaP cells stably infected with indicated CRISPR/shRNA [false discovery rate (FDR)± 0.1]. RNA sequencing was analyzed by Partek. **G,** Top, volcano plot showing the genes altered in LNCaP cells stably coinfected with *BRCA2* CRISPR and *RB1* shRNA compared with scrambled gRNA- scrambled shRNA (scr)–infected LNCaP cells. Bottom, the bar graph represents the disease-specific pathway analysis of the genes unregulated in *BRCA2-RB1* knockout/knockdown LNCaP cells. Pathway analyses were performed using ToppGene. **H,** *BRCA2-RB1* signature score (see Materials and Methods) generated from the 10 most upregulated (top) or downregulated (bottom) genes in LNCaP-*BRCA2-RB1* cells compared with control LNCaP cells from the RNA sequencing (**F**) and converted into an mRNA score using ssGSEA. Clinical significance of *BRCA2-RB1* score determined by biochemical recurrence–free survival in Taylor primary prostate cancer cohort ($n = 131$). Log-rank test was used to compare groups.

Downloaded from http://aacrjournals.org/clincancerres/article-pdf/26/8/2047/2067287/2047.pdf by guest on 27 August 2022

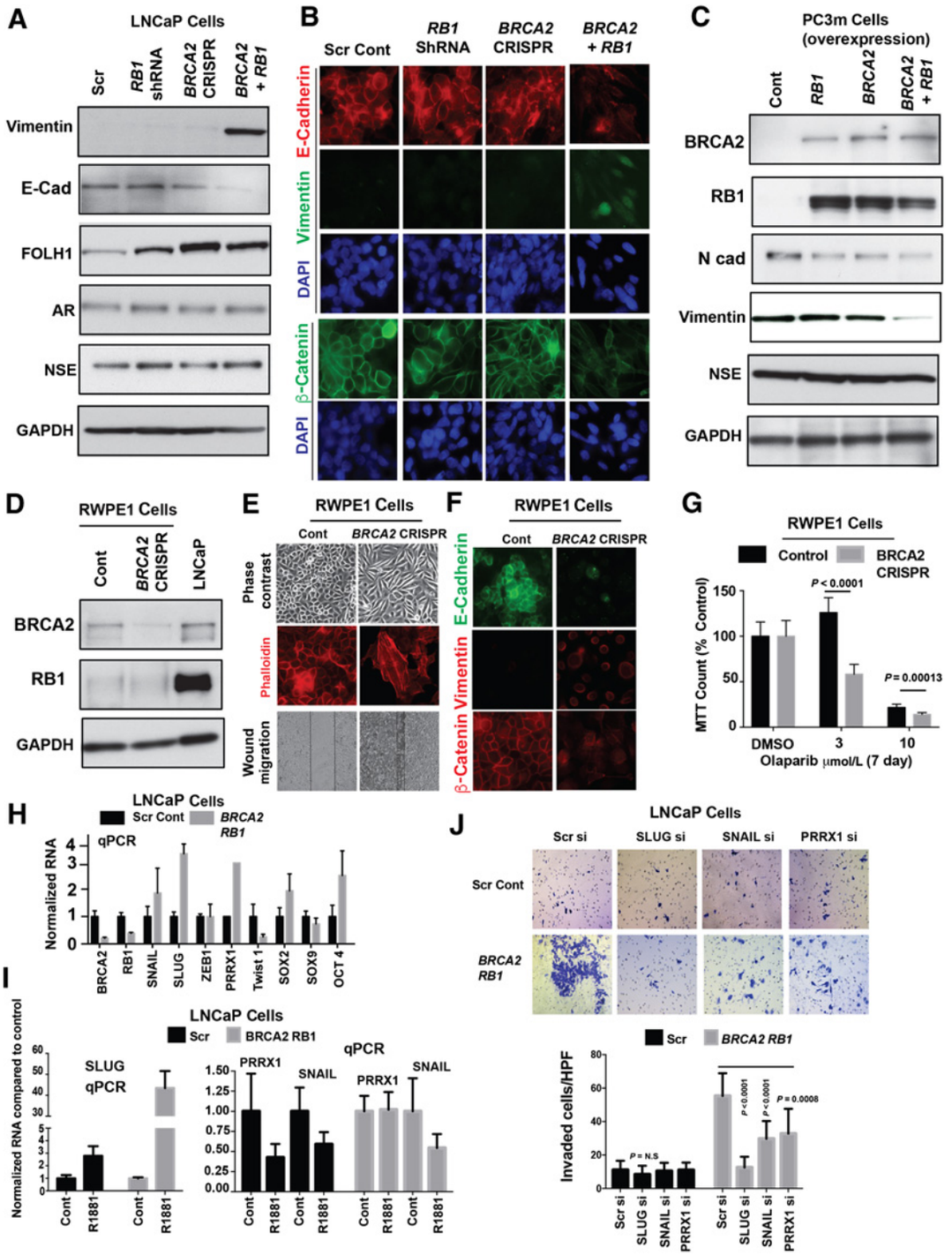

Figure 3.

Induction of EMT phenotype resulted in co-loss of *BRCA2* and *RB1* phenotype in LNCaP cells. **A,** Western blot showing indicated protein levels in LNCaP-*BRCA2* CRISPR-edited (CRISPR gRNA 2) and nontargeting gRNA-infected control (Scr-CRISPR) cells infected with lentiviral *RB1* short hairpin RNA (shRNA). Scr-CRISPR and *BRCA2*-CRISPR2 cells were also transfected with nontargeting shRNA (scr-Sh) for control of shRNA. GAPDH served as the loading control. **B,** Immunofluorescence (400× magnification) of E-cadherin, vimentin, and β-catenin on indicated CRISPR/shRNA knockdown and scrambled CRISPR control LNCaP cells. Nuclei were stained with DAPI (blue). Note that LNCaP-*BRCA2-RB1* cells exhibit significant loss of cell surface E-cadherin and β-catenin but exhibit gain of vimentin compared with scrambled CRISPR control LNCaP cells. **C,** *BRCA2* and/or *RB1* transiently overexpressed in PC3M cells. Control cells were transfected with empty vector. Western blot shows expression of indicated proteins. GAPDH served as the loading control. **D,** Western blot showing *BRCA2* and *RB1* levels in RWPE1-*BRCA2* CRISPR-edited (CRISPR gRNA 2) and nontargeting gRNA-infected control cells. LNCaP cells were used as control. (*Continued on the following page.*)

Downloaded from http://aacrjournals.org/clincancerres/article-pdf/26/8/2047/2067287/2047.pdf by guest on 27 August 2022

enrichment of the hallmark EMT signaling pathway (Supplementary Fig. S3A; Supplementary Table S4). We observed decreased expression of E-cadherin and increased expression of the mesenchymal marker vimentin (both translational and transcriptional) in the double knocked down cells compared with control LNCaP cells (**Fig. 3A**; Supplementary Fig. S3B). Our immunofluorescence staining also showed loss of cell membrane E-cadherin and β–catenin and gain of vimentin in the LNCaP-*BRCA2-RB1* cells (**Fig. 3B**). This observation is consistent with the elongated morphology and actin cytoskeleton remodeling of LNCaP-*BRCA2-RB1* cells (**Fig. 2C**). Moreover, these findings further supported the observation that LNCaP-*BRCA2-RB1* cells undergo an EMT-like transformation, while knockdown of *BRCA2* or *RB1* alone induce a partial EMT-like phenotype (**Fig. 3A** and **B**). However, we did not find any changes in expression of AR or the neuroendocrine marker NSE in double knockout/knockdown LNCaP cells compared with control cells (**Fig. 3A**).

We overexpressed *BRCA2* and *RB1* in highly aggressive mesenchymal-like PC3M cells that exhibit low endogenous *BRCA2* and *RB1*. Overexpression of *BRCA2* and *RB1* inhibits vimentin and N-cadherin expression in PC3M cells; however, NSE expression remains unchanged (**Fig. 3C**). Interestingly, we also observed that overexpression of either of the genes (*BRCA2* or *RB1*) autoregulates the expression of the other in PC3M cells (**Fig. 3C**), further indicating the feed-forward loop between *BRCA2* and *RB1* in prostate cancer. *BRCA2* and *RB1* also exhibit diminished Boyden chamber migration and Matrigel invasion in overexpressed PC3M cells compared with control cells (Supplementary Fig. S3D).

To further validate whether loss of *BRCA2* and *RB1* is sufficient to induce EMT in prostate cancer cells, we used the immortalized benign human prostate cells RWPE1. RWPE1 cells express significantly lower RB1 protein compared with parental LNCaP cells due to their expression of a single copy of human papilloma virus 18 (HPV 18; **Fig. 3D**; ref. 45). We used CRISPR to knockout *BRCA2* from RWPE1 cells (**Fig. 3D**) and observed that *BRCA2* from knockout RWPE1 cells exhibit elongated morphology and remodeling of actin filament (**Fig. 3E**). We also observed enhanced wound migration in *BRCA2* knockout RWPE1 cells (**Fig. 3E**). Our immunofluorescence staining also showed loss of cell membrane E-cadherin and β catenin and gain of vimentin in the *BRCA2*-knockout RWPE1 cells (**Fig. 3F**). As predicted, *BRCA2*-null RWPE1 cells also exhibited enhanced sensitivity to PARPi olaparib (**Fig. 3G**).

We analyzed the transcriptome that is enriched in the *BRCA2-RB1* codeleted TCGA provisional prostate cancer cohort and performed GSEA hallmark pathway analyses (Supplementary Table S5). We observed that EMT is one of the common pathways enriched in the *BRCA2-RB1*–null cell line and TCGA cohort (Supplementary Fig. S3C). More importantly, our analysis of the Setlur prostate cancer cohort (lethal vs. indolent) using Oncomine suite and GSEA also demonstrated enrichment [$P = 0.015$, q (P_{adj} value based on FDR) = 0.039, normalized enrichment score (NES) = 1.764] of the EMT pathway (Supplementary Fig. S3F; Supplementary Table S6), indicating the clinical significance of EMT in lethal prostate cancer.

To determine which transcriptional factors were involved in EMT transformation, we analyzed the expression of previously demonstrated EMT-related transcription factors by qPCR (**Fig. 3H**). We observed upregulation of EMT transcription factors *SLUG* (SNAI2) and *SNAIL* (SNAI1) and transcriptional coactivator *PRRX1* in LNCaP-*BRCA2-RB1* compared with LNCaP cells (**Fig. 3H**). Relative SLUG expression was significantly (>100-fold) higher compared with other EMT transcription factors in LNCaP-*BRCA2-RB1* cells (**Fig. 3I**). Previously *SLUG* had been demonstrated as an androgen-regulated transcription factor that facilitates castration resistance in prostate cancer (46). We observed that treatment with androgen (R1881) significantly increased *SLUG*, but not *SNAIL* or *PRRX1* mRNA in LNCaP-*BRCA2-RB1* cells (**Fig. 3I**). We showed that siRNA-mediated knockdown of *SLUG*, *SNAIL*, or *PRRX1* inhibits invasiveness compared with control siRNA–transfected LNCaP-*BRCA2-RB1* cells or control (scr) LNCaP cells (**Fig. 3J**).

Frequent deletion of *BRCA2* in prostate cancer

We analyzed *BRCA2* status in a pan-cancer dataset derived from cBioPortal for Cancer Genomics (23, 24) where *BRCA2* is frequently altered (*BRCA2* alteration frequency >5% of cases; number of cases >50; Supplementary Fig. S4A). We observed more frequent homozygous deletions of *BRCA2* in prostate cancer (localized and mCRPC) than in other cancers (whereas other cancers exhibit frequent mutational events; Supplementary Fig. S4A). In the Armenia and colleagues' prostate cancer dataset, which contains both primary (localized) and mCRPC cases (26), we observed *BRCA2* alterations in approximately 10% of mCRPC cases compared with only approximately 2.5% in primary cases ($P = 2.91e-06$; summarized in Supplementary Table S7). *BRCA2* alterations are more common than other major DDR pathway components, and are enriched in mCRPC relative to localized disease, suggesting it is associated with, if not a driver of, aggressive disease (**Fig. 4A**; Supplementary Table S7). Note that the Armenia cohort was not designed to determine germline mutations of DDR pathway components.

Further in-depth analysis of the *BRCA2* status in multiple independent publicly available and published prostate cancer datasets (from cBioPortal) revealed that a significant fraction of localized as well as metastatic cases exhibit deletion (homozygous and heterozygous) of *BRCA2*, which had not been previously

(*Continued.*) GAPDH served as the loading control. Note that RWPE1 cells exhibit significantly depleted RB1 protein compare with LNCaP cells. **E,** Top, phase contrast bright field micrograph (200× magnification) showing the morphology of RWPE1 cells after infection with *BRCA2* CRISPR. Middle, immunofluorescence (400× magnification) of f-actin filament stained with phalloidin in indicated *BRCA2* CRISPR–infected RWPE1 cells. Nuclei were stained with DAPI (blue). Note that RWPE1-*BRCA2* cells exhibit cytoskeleton rearrangement compared with control RWPE1 cells. Bottom, micrographs (in 40× magnification) of 24-hour wound migration of indicated cells (see Materials and Methods). **F,** Immunofluorescence (400× magnification) of E-cadherin, vimentin, and β-catenin on *BRCA2* CRISPR–infected RWPE1 and CRISPR control RWPE1 cells. Note that RWPE1-*BRCA2* cells exhibit significant loss of cell surface E-cadherin and β-catenin but exhibit gain of vimentin compared with control RWPE1 cells. **G,** *BRCA2* CRISPR–infected RWPE1 and CRISPR control RWPE1 cells were treated with 3 μmol/L and 10 μmol/L olaparib for 7 days. Equivalent volume of DMSO was used as placebo treatment. Cell growth was measured by MTT assay; SD, *P* values determined by Student *t* test. **H,** The bar graph shows the changes (via qPCR) of selected EMT and stem cell markers after coelimination of *BRCA2* and *RB1* in LNCaP cells, compared with scrambled control cells. LNCaP-*BRCA2-RB1* or control cells were incubated in charcoal-stripped medium (CSS) for 24 hours followed by treatment with 1 nmol/L R1881 for another 48 hours (in CSS). **I,** The bar graph shows the changes (via qPCR) of SLUG and PRRX1 in treated and untreated cells. Expression of the indicated genes normalized with untreated control and GAPDH. **J,** *SLUG, SNAIL*, and *PRRX1*- or scrambled SMARTpool siRNA-transfected LNCaP-*BRCA2-RB1* or scrambled LNCaP cells. A total of 2.5×10^3 indicated cells (72 hours after indicated siRNA transfection) were plated on the top of Boyden chamber in serum-free media; 10% serum in the bottom chamber was used as chemoattractant. After 24 hours, cells in the lower side of the chamber were fixed, stained, photographed in 100× magnification (top), and counted and represented in the form of the bar graph (bottom). *P* values were determined by Student *t* test.

Downloaded from http://aacrjournals.org/clincancerres/article-pdf/26/8/2047/2067287/2047.pdf by guest on 27 August 2022

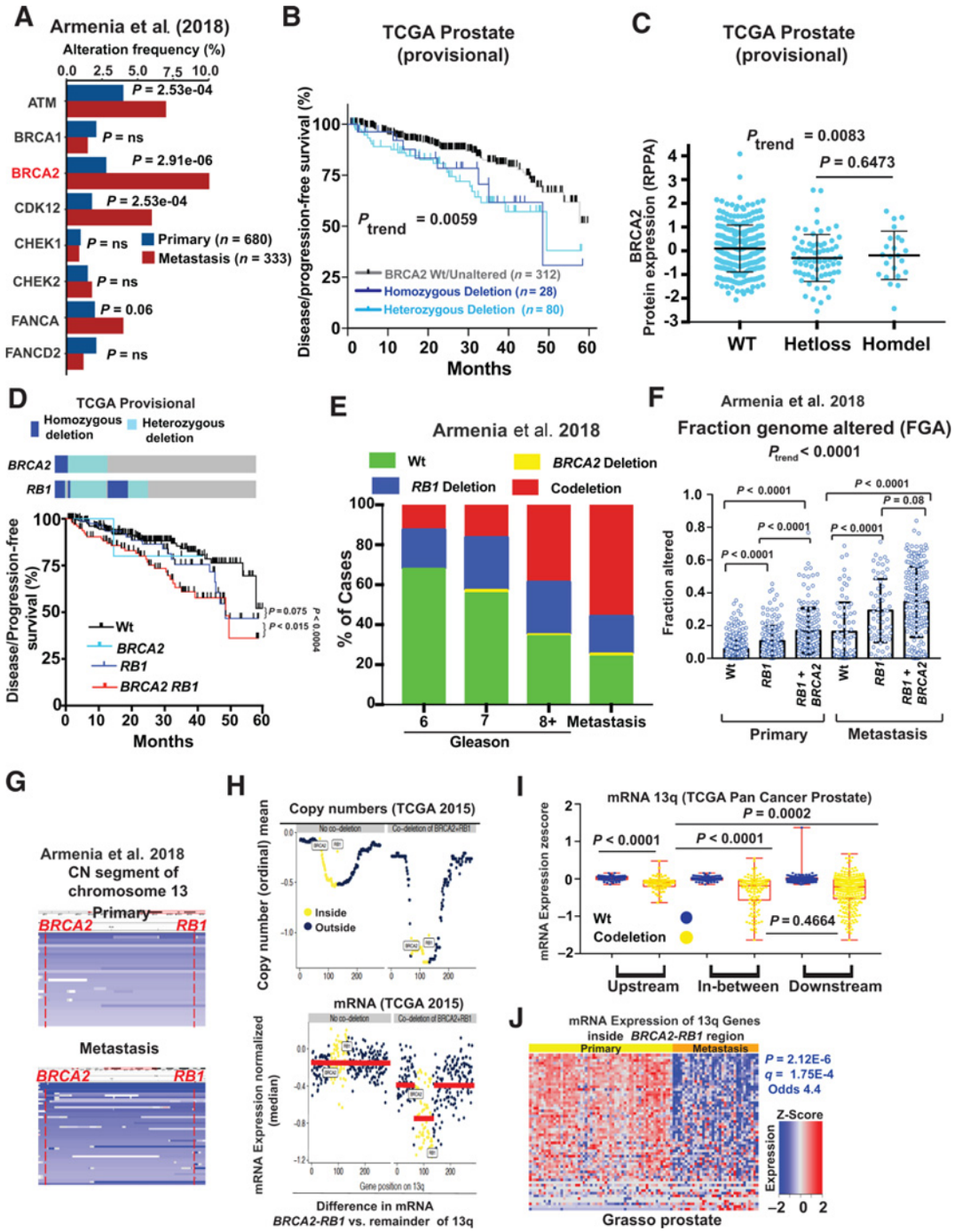

Figure 4.

Concomitant deletion of *BRCA2* and *RB1* represents an aggressive variant of prostate cancer. **A,** Alteration frequency of various DDR components in the Armenia and colleagues' cohort; *P* values calculated by Fisher exact test. **B,** Significance of *BRCA2* alteration (either homozygous or heterozygous deletion) and disease/progression-free survival (5 years) in TCGA provisional cohort (primary prostate cancer). Kaplan–Meier curves were calculated for *BRCA2* wild-type (wt) (diploid + chromosomal gain) and *BRCA2* homozygous or heterozygous deletion; the log-rank test was used to compare groups and to determine the significance. **C,** Association between BRCA2 protein expression [reverse-phase protein arrays (RPPA)] and genomic deletion in TCGA cohort; *P* value (±SD) and P_{trend} determined by one-way ANOVA. **D,** Top, codeletion (homozygous or heterozygous) of *BRCA2* and *RB1* in TCGA provisional cohort. Note that *BRCA2* is frequently deleted with *RB1*. Bottom, significance of codeletion of *BRCA2* and *RB1* was determined by disease/progression-free survival in patients with primary prostate cancer in the TCGA provisional cohort. Kaplan–Meier curves for 60 months were defined for each group. Log-rank test was used to compare groups. **E,** Higher rates of codeletion of *BRCA2* and *RB1* and higher risk in primary tumors and advanced-stage disease. Gleason grade and metastatic status are shown by alteration status in the Armenia and colleagues' cohort; *P* value calculated by Fisher exact test (Supplementary Table S8). (*Continued on the following page.*)

Downloaded from http://aacrjournals.org/clincancerres/article-pdf/26/8/2047/2067287/2047.pdf by guest on 27 August 2022

described (Supplementary Fig. S4B). Our analysis also revealed that *BRCA2* alterations (homozygous or heterozygous deletions, as well as mutations, denoted as *BRCA2* alterations throughout this study) were significantly enriched ($P = 0.0216$) in this combined mCRPC dataset ($n = 444$) compared with a primary (localized) dataset ($n = 925$; Supplementary Fig. S4B). While the TCGA provisional cohort was not designed to look at clinical outcomes (overall survival), in the available data, *BRCA2* deletion is significantly associated with shorter disease/progression-free survival (5 years; $P_{trend} = 0.0059$; **Fig. 4B**). Interestingly, we are unable to detect any difference in disease progression between patients with homozygous and heterozygous *BRCA2* deletions (**Fig. 4B**). Our observation suggests that even heterozygous loss of *BRCA2* may be associated with a more aggressive form of prostate cancer.

Homozygous and even heterozygous deletion of *BRCA2* significantly reduced BRCA2 protein levels as determined by reverse-phase protein array (RPPA; $P_{trend} = 0.0083$; **Fig. 4C**). We were unable to detect any difference in BRCA2 protein expression between heterozygous and homozygous cases (**Fig. 4C**). However, in the same TCGA prostate cancer cohort, we did not detect a relationship between *BRCA2* deletion (either homozygous or heterozygous) and *BRCA2* mRNA expression (Supplementary Fig. S4C). Heterozygous deletion of *BRCA2* is sufficient to reduce protein level but not mRNA level, indicating that single copy loss may lead to haploinsufficiency of BRCA2 protein expression. Decreased BRCA2 protein expression is significantly correlated with shorter disease-free survival (Supplementary Fig. S4D). Taken together, for the first time we demonstrate the potential clinical significance of heterozygous deletion of *BRCA2* in primary prostate cancer through loss of BRCA2 protein expression.

BRCA2 is frequently codeleted with *RB1* in aggressive prostate cancer

A prior sequencing study revealed that codeletion (heterozygous and homozygous) of *RB1* and *BRCA2* is present in a significant fraction of primary prostate cancers [∼25% in TCGA provisional cohort (**Fig. 4D**, top); ref. 35]. Interestingly, in the MSK-IMPACT prostate cancer cohort (36), we observed that *BRCA2* homozygous deletion, not mutation, is enriched in metastatic cases and cooccurs with homozygous *RB1* deletion (Supplementary Fig. S4E). In the TCGA and Taylor prostate cancer datasets, patients with primary prostate cancer who have *BRCA2-RB1* codeletion have significantly shorter disease/progression-free survival compared with patients with deletion of neither or of *RB1* alone (**Fig. 4D** bottom; Supplementary Fig. S4H, bottom), while deletion of *BRCA2* without *RB1* is rare (**Fig. 4D**, top; Supplementary Fig. S4H, top). Also, *BRCA2* copy number and *RB1* copy number are correlated in both primary prostate cancer (TCGA) and mCRPC (Kumar) cohorts (Supplementary Fig. S4F). However, note that unlike *BRCA2, RB1* mRNA expression is significantly associated with *RB1* genomic deletion (heterozygous and homozygous) in primary (TCGA) and mCRPC (Kumar) cohorts (Supplementary Fig. S4G).

Codeletion of *BRCA2-RB1* is significantly enriched in high Gleason grade prostate cancer as well as in metastases (**Fig. 4E**; Supplementary Table S8). However, deletion of *RB1* alone is not significantly associated with stage or progression to metastasis (**Fig. 4E**). The details of the codeletion and *P* values of each stage are summarized in Supplementary Table S8. We also observed that approximately 10% of low-grade (Gleason 6) cases harbor genomic codeletion of *BRCA2* and *RB1* (Supplementary Fig. S4I). We established the mRNA expression of the genes that are upregulated due to codeletion of *BRCA2* and *RB1* in Gleason 6 disease in TCGA provisional prostate cancer cohort (Supplementary Fig. S4I; Supplementary Table S9). To further assess the importance of the *BRCA2-RB1* codeletion in low-grade primary prostate cancer, we compared the *BRCA2-RB1* loss Gleason 6 gene signature from TCGA to the metastatic prostate cancer signature using Oncomine suite (25). In the Taylor cohort, we observed enrichment of this *BRCA2-RB1* loss Gleason 6 gene signature in metastatic prostate cancer ($P = 2.00E-20$, odds 3.7; Supplementary Fig. S4I).

We extended our study to matched (localized and metastatic) prostate cancer samples in the Kumar and colleagues cohort to further assess the direct association between codeletion of both genes and metastatic progression. Supplementary Table S10 displays the 12 patients with mCRPC in the Kumar and colleagues cohort that had matched localized and metastatic samples. All 8 patients (66.7%) who had codeletion of *BRCA2* and *RB1* in their localized tumors retained their *BRCA2-RB1* codeletion in all of their metastatic tumors (Supplementary Table S10), indicating that this codeletion may be critical to metastatic progression. Interestingly, for the one patient (06-081) who had an *RB1* deletion alone in his localized prostate tumor, the *RB1* deletion was not seen in all his metastatic tumors. These data suggest that codeletion of *BRCA2* and *RB1* in primary disease is likely a driver to mCRPC.

In an analysis of the Armenia and colleagues' dataset, which contains both primary and mCRPC cases, we found that *BRCA2-RB1* co-loss in early prostate cancer appeared to be significantly associated with increased fraction of genome altered (**Fig. 4F**). Fraction of genome altered is a biomarker associated with genomic instability and also appears to be associated with prostate tumor aggressiveness (47), suggesting that *BRCA2-RB1*–null tumors are likely aggressive in nature.

Deletion of *BRCA2-RB1* region of chromosome 13q in prostate cancer

Copy number segment analysis of primary and mCRPC samples from the Armenia and colleagues' dataset indicated frequent deletion of the *BRCA2-RB1* region of chromosome 13q (**Fig. 4G**). We also observed copy number loss of other genes located in the *BRCA2-RB1* region in patients who harbored the codeletion of *BRCA2* and *RB1*

(*Continued.*) **F,** Fraction of genome alteration (FGA) in patients with prostate cancer with *BRCA2* and/or *RB1* deletion was analyzed from primary and metastatic cases in Armenia and colleagues' 2018 prostate cancer cohort (±SD); individual blue circles indicate individual patients. Because of the very low number of cases with *BRCA2* deletion only, those patients are not shown on this graph. *P* values determined by Student *t* test; P_{trend} values determined by one-way ANOVA. **G,** Copy number (CN) segment analysis of *BRCA2-RB1* region of chromosome 13q in Armenia and colleagues' cohort. Samples are divided into primary and metastatic prostate cancer. **H,** Copy number (top) and mRNA expression (bottom) of the chromosome 13q genes in TCGA 2015 cohort. Genes located in the region between *BRCA2* and *RB1* indicated as yellow and outside this region marked as blue. Median expression of mRNA indicated by red line. **I,** Comparison between mean mRNA expression of the 13q genes in patients with prostate cancer. The transcriptomic analyzed data from TCGA pan-cancer prostate cohort. Parents harboring *BRCA2-RB1* codeletion indicated as yellow and unaltered indicated as blue. The genes are divided in three groups on the basis of their chromosomal position [upstream from *BRCA2* ($n = 69$), in the region between *BRCA2* and *RB1* ($n = 63$), or downstream from the *BRCA2-RB1* region ($n = 150$; ±SD)]; *P* values determined by Student *t* test. Each point represents a single gene. **J,** Heatmap (hierarchical clustering) of the mRNA expression of 63 genes (*BRCA2-RB1* region of chromosome 13q) in primary and mCRPC samples in Grasso cohort. The heatmap is generated in Oncomine suite. Genes are ranked on the basis of *P* value and fold changes.

Downloaded from http://aacrjournals.org/clincancerres/article-pdf/26/8/2047/2067287/2047.pdf by guest on 27 August 2022

(**Fig. 4H**, top). To further assess the nature of this deletion, we analyzed the mRNA of all the protein-coding genes on chromosome 13q (**Fig. 4H**, bottom; Supplementary Table S11). We observed that the mRNA expression of chromosome 13q genes between *BRCA2* and *RB1* was lower in *BRCA2-RB1*–deleted patients compared with wild-type patients in the TCGA 2015 cohort (**Fig. 4H**). More in-depth analysis in the TCGA pan-cancer prostate cohort (extended TCGA 2015 cohort) showed that the mRNA expression of genes located downstream of *BRCA2* was significantly lower than for genes located upstream of *BRCA2* in patients who harbored a codeletion of *BRCA2* and *RB1* (**Fig. 4I**). These data indicate an interstitial deletion of the *BRCA2-RB1* region in prostate cancer rather than deletion of the entire chromosome 13q arm.

We observed an association between the loss of mRNA expression of *BRCA2-RB1* region genes in the mCRPC cohorts compared with primary (localized) prostate cancer. Loss of expression of these genes was seen (to a greater degree) in mCRPC compared with primary cases in the Grasso ($P = 2.12E-6$, OR 4.4) and Taylor ($P = 2.47E-20$, OR 12.2) cohorts (Grasso: primary $n = 59$, mCRPC $n = 35$; Taylor primary $n = 131$, mCRPC $n = 19$; **Fig. 4J**; Supplementary Fig. S4J). Note that in the Grasso cohort, the mCRPC specimens were isolated by rapid autopsy from metastatic sites (30). Taken together, these data suggest that an interstitial deletion of the *BRCA2-RB1* region of chromosome 13q may be associated with castration resistance and metastasis.

Castration-resistant aggressive human prostate cancer cells exhibit genomic codeletion of *BRCA2* and *RB1*

To further confirm that in prostate cancer *BRCA2* is frequently deleted with *RB1* rather than alone, we developed a 3-color FISH probe to apply to human cells. We validated our probes on human peripheral blood and immortalized prostate cells (RWPE-1), in which almost every cell exhibits two copies of *BRCA2* and *RB1* (**Fig. 5A** and **C**; Supplementary Fig. 5A; Supplementary Table S12). Human CRPC cell lines E006AA, DU145, PC3, and PC3M exhibited uniform heterozygous codeletion of *BRCA2* and *RB1* (**Fig. 5A**; Supplementary Fig. S5A; Supplementary Table S12). Heterozygous codeletion of *BRCA2* and *RB1* is associated with high fraction of genome altered in PC3 and DU145 cells, but not in 22RV1 and MDA PC2B cells (absence of codeletion) or in LNCaP cells (partial codeletion) in The Cancer Cell Line Encyclopedia (ref. 48; **Fig. 5B**). The detailed analysis of the *BRCA2-RB1* copy number and ploidy of individual prostate cancer cell lines is shown in Supplementary Table S12. Most importantly, we were able to detect heterozygous codeletion of *BRCA2* and *RB1* in VCaP cells (not noted in sequencing study), which also display a high fraction of genome altered (**Fig. 5A** and **B**; Supplementary Fig. S5A).

We found that approximately 60% of parental LNCaP cells harbor loss of one or more copies of *RB1*, including approximately 10% with codeletion of *BRCA2* (**Fig. 5A–C**; Supplementary Table S12). We observed heterogeneity in chromosome number (ploidy, 2–10 copies of chromosome/cell) in LNCaP cells indicating the heterogeneous nature of the parental LNCaP cell line (**Fig. 5D**; Supplementary Table S12). Previous studies have identified a castration-resistant low-PSA subpopulation among parental LNCaP cells (49). This is consistent with our current observation and suggests the clonal expansion of a subpopulation of LNCaP cells in the castrate environment as demonstrated previously (49). Interestingly, the LNCaP-derived hormone-independent LNCaP-Abl cell line (able to grow in androgen-independent culture condition) exhibits uniform co-loss of 1 of 4 copies of *BRCA2* and *RB1*, further indicating this codeletion is directly associated with ADT resistance and also may indicate a clonal expansion of castration-resistant *BRCA2-RB1*–deleted population from parental LNCaP cells (**Fig. 5A**, **C**, and **D**; Supplementary Table S12).

In these cell lines, the protein and mRNAs of both genes were consistently decreased (**Fig. 5E**; Supplementary Fig. S5B). Although the castration-resistant LNCaP subclone C42 exhibits uniform heterozygous deletion of *RB1* only, attenuation of *BRCA2* protein and mRNA is observed as well. This indicates that an additional mechanism of loss of *BRCA2* in *RB1*-deleted cells may lead to the castration-resistant phenotype (**Fig. 5A** and **E**; Supplementary Fig. S5B; Supplementary Table S12).

Our immunoblot analysis showed that the human CRPC cell lines DU145, PC3, and the PC3-derivative PC3M that exhibited uniform heterozygous codeletion of *BRCA2* and *RB1* (**Fig. 5A**; Supplementary Fig. S5A; Supplementary Table S12) also exhibit the EMT-like phenotype, including upregulation of vimentin and loss of E-cadherin expression (**Fig. 5F**). However, LAPC4, 22RV1 (mutant *BRCA2* but wild-type *RB1*), and LNCaP (*RB1* partial deletion but wild-type *BRCA2*) exhibit more epithelial-like characteristics (refs. 34, 48; **Fig. 5F**). Codeletion of *BRCA2-RB1* in LNCaP-Abl cells is also associated with upregulation of vimentin protein expression, which is consistent with our current observations (**Fig. 5F**).

Codeletion of *BRCA2-RB1* in the LNCaP-Abl cell line is consistently associated with sensitivity to various PARPi (rucaparib and talazoparib) and platinum drugs compared with parental LNCaP cells (**Fig. 5G**). Note that although parental LNCaP cells harbor several defects in various DDR genes (Supplementary Fig. S5C), the LNCaP subline LNCaP-Abl exhibits more PARPi-mediated cell growth inhibition compared with parental LNCaP cells (**Fig. 5G**). Although the COSMIC cancer cell line dataset showed that LNCaP cells harbor a deletion-frameshift mutation of *BRCA2* (p.D946fs*14), sequencing studies from The Cancer Cell Line Encyclopedia (**Fig. 5B**; ref. 48) and the Taylor prostate dataset (34) were unable to detect such *BRCA2* mutation in parental LNCaP cells. A prior study also showed that LNCaP cells express a wild-type *BRCA2* transcript (50). These data suggest that heterozygous codeletion of *BRCA2* and *RB1* in LNCaP-Abl cells is sufficient to reduce the mRNA expression of both genes and therefore induce sensitivity to PARPi (**Fig. 5G**). Similarly, PC3M cells, which also harbor genomic codeletion of *BRCA2* and *RB1*, show sensitivity to various PARPi or platinum drugs (Supplementary Fig. S5D, bottom). In contrast, we have observed that the 22RV1 cell line, which harbors a T3033Nfs*11 mutation in *BRCA2*, showed sensitivity to cisplatin and modest sensitivity to talazoparib, but not to other PARPi (Supplementary Fig. S5D, top). Taken together, these results indicate that co-loss of *BRCA2-RB1* is a cell line–independent event and is frequently associated with castration resistance and leads to heightened sensitivity to PARPi.

Organoids derived from human patients with mCRPC harbor coheterozygous deletion of *BRCA2 and RB1*

3D organoid cultures of human cancers have shown extreme promise in cancer research (21, 51–53). Organoids can potentially be used as avatars for human cancer to study the molecular mechanisms of candidate genes and the effect of drugs. Earlier prostate organoids (MSK-PCa 1–7) were successfully developed from patients with CRPC. These organoids successfully retain the genetic characteristics of patients and grow *in vitro* as well as in immunodeficient mice (21). We tested the *BRCA2-RB1* status by 3-color FISH in three mCRPC organoids that were originally isolated from metastatic sites from castration-resistant tumors (21). As a control, we also analyzed a benign prostate organoid by FISH. We observed that organoid

Downloaded from http://aacrjournals.org/clincancerres/article-pdf/26/8/2047/2067287/2047.pdf by guest on 27 August 2022

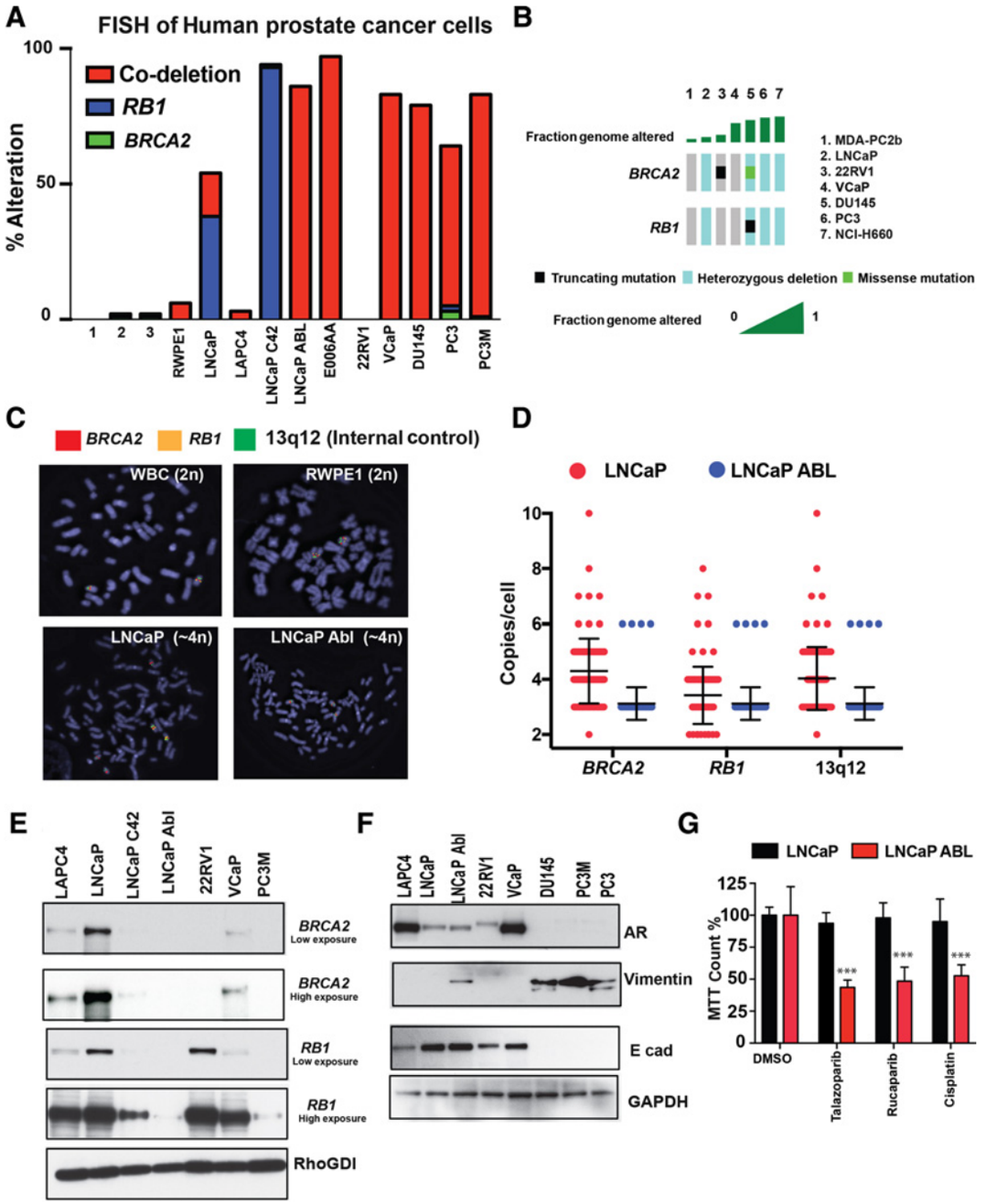

Figure 5.

Concomitant heterozygous codeletion of *BRCA2-RB1* in prostate cancer cell lines. **A,** FISH analysis of indicated human prostate cancer cell lines using 3-color probes. The bar graph shows the deletion of *BRCA2* and/or *RB1* per 100 cells. Normal peripheral blood cells and RWPE1 cells were used as controls. **B,** *BRCA2* and *RB1* status in various prostate cancer cell lines in The Cancer Cell Line Encyclopedia. **C,** Micrographs of FISH analysis of indicated human prostate cancer cell lines using a 3-color probe (red: BRCA2; orange: RB1; green: 13q 12, internal control). **D,** The graph represents the copies of BRCA2, RB1, and 13q LNCaP cells analyzed by the 3-color FISH. Each point represents a single cell. A total of 100 individual cells from each cell line were counted and represented graphically. **E,** *BRCA2* and *RB1* protein expression in various prostate cancer cell lines was analyzed by Western blot analysis. RHoGDI was used as loading control. **F,** Expression of the androgen receptor, vimentin, and E-cadherin in human prostate cancer cells analyzed by Western blots. GAPDH was used as loading control. **G,** LNCaP and LNCaP-Abl cells were treated with a PARPi [rucaparib (500 nmol/L) or talazoparib (5 nmol/L)] or cisplatin (500 nmol/L) for 4 days. DMSO was used as a control. The graph shows cell growth measured by MTT assay (±SD); *P* values determined by Student *t* test (***, $P < 0.001$).

Downloaded from http://aacrjournals.org/clincancerres/article-pdf/26/8/2047/2067287/2047.pdf by guest on 27 August 2022

MSK-PCa1 and MSK-PCa3 exhibited heterozygous co-deletion (~100% of cells) of *BRCA2* and *RB1;* however, MSK-PCa2 largely (94%) exhibited heterozygous deletion of *RB1* only (**Fig. 6A** and **B**; Supplementary Fig. S6A; Supplementary Table S13). The copy number segment analysis of the prostate cancer organoids matched the FISH analysis, showing codeletion of *BRCA2* and *RB1* in MSK-PCa1 and MSK-PCa3, and deletion of *RB1* only in MSK-PCa2. Heterozygous deletion of *BRCA2* and *RB1* is consistent with loss of their protein expression (**Fig. 6C**) as identified in our previous observation in TCGA prostate cancer cohort (**Fig. 4C**). We did observe upregulation of BRCA2 protein expression in the MSK-PCa2 organoid, which may be due to an extra copy of chromosome

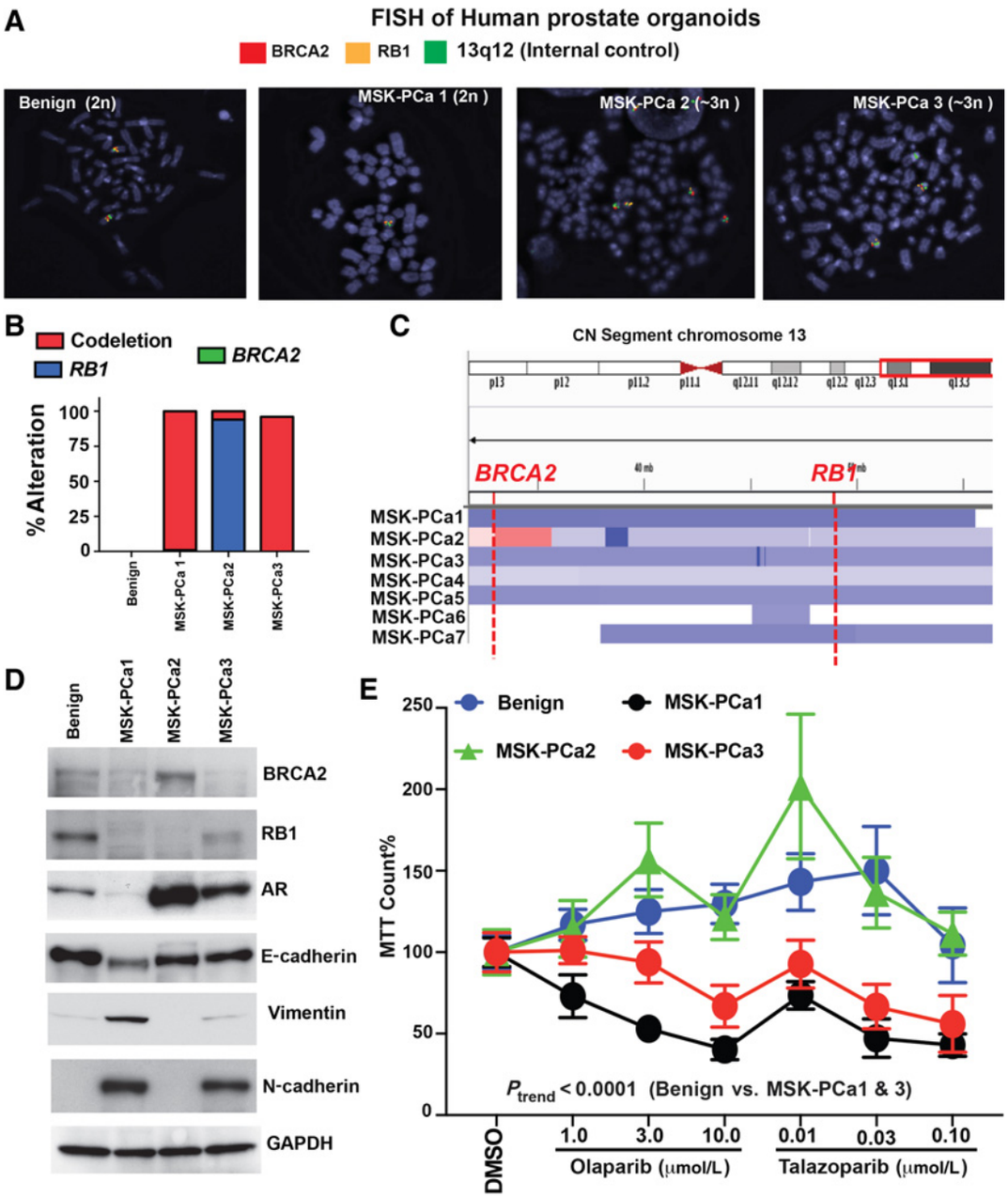

Figure 6.

Organoids derived from patients with mCRPC represent an experimental model for *BRCA2-RB1* codeletion. **A,** FISH analysis of indicated mCRPC-derived organoids (MSK-PCa 1–3) and benign prostate organoids using 3-color probes (see Materials and Methods). **B,** The bar graph shows the deletion of *BRCA2* and/or *RB1* per 100 cells. Near-diploid benign prostate organoid is used as a control. **C,** Copy number (CN) segment analysis of *BRCA2-RB1* region of chromosome 13q in mCRPC organoids. **D,** Western blot showing indicated protein levels in human mCRPC organoids. GAPDH served as the loading control. **E,** Organoids were treated with PARPi (olaparib and talazoparib) in indicated concentrations for 3 days. The graphs show cell growth measured by MTT assay (±SD); *P* trends determined by two-way ANOVA.

Downloaded from http://aacrjournals.org/clincancerres/article-pdf/26/8/2047/2067287/2047.pdf by guest on 27 August 2022

13 (Supplementary Fig. S6A; Supplementary Table S13) rather than due to transcriptional activity of *BRCA2*. MSK-PCa1 and MSK-PCa3 also showed upregulation of mesenchymal markers N-cadherin and vimentin (the latter only in MSK-PCa1), indicating the EMT-like phenotype of these cells (**Fig. 6D**). However, MSK-PCa2 exhibited more epithelial morphology (**Fig. 6D**). We also observed higher *SNAIL* and *PRRX1* mRNA expression in the MSK-PCa1 organoid (Supplementary Fig. S6C).

We observed growth reduction of MSK-PCa1 and MSK-PCa3 compared with the benign organoid when treated with the PARPi olaparib and talazoparib (**Fig. 6E**). However, PARPi did not have an inhibitory effect on the growth of the MSK-PCa2 organoid. Interestingly, none of the organoids harbored any other known mutation in DDR genes (Supplementary Fig. S6B), indicating that coheterozygous deletion of *BRCA2* and *RB1* is sufficient to sensitize cells to PARPi treatment–mediated growth inhibition.

We observed *BRCA2-RB1* deletion (heterozygous and homozygous) in approximately 30% of all cancer types determined from TCGA pan-cancer cohort (without prostate cancer $n = 10{,}820$; Supplementary Fig. S6D, top; Supplementary Table S14). We observed that deletion of either *BRCA2* or *RB1* or codeletion is associated with shorter overall survival ($P_{\text{trend}} < 0.0001$; Supplementary Fig. S6D, bottom), indicating that loss of *BRCA2* or *RB1* alone may also play an important role in disease progression in the pan-cancer scenario.

Discussion

Mutations in *BRCA2*, a DDR and cancer susceptibility gene, have been known to confer elevated risk of breast and ovarian cancer, and *BRCA2* mutations are prevalent in men with advanced prostate cancer (1). In fact, pathologic variants in DDR pathway genes are prevalent in a substantial subset of men who develop mCRPC. Compared with other DDR pathway components, alterations of *BRCA2* have been observed in a higher proportion of men with mCRPC and they are associated with a worse prognosis, especially when the mutations involve loss of gene function (2, 3). In the PROREPAIR-B mCRPC cohort (of 419 patients, 68 had germline DDR mutations, including 14 with *BRCA2* mutations), *BRCA2* germline mutations were reported to have a deleterious impact on mCRPC outcome (54). Furthermore, integrative whole genome and transcriptome analysis in 101 samples from patients with mCRPC identified deletion (homozygous and heterozygous) of *BRCA2* in a significant number of men (55). Several other studies also measure DDR and *BRCA2* alteration and confirm a high prevalence. Herein, we observed that *BRCA2* and its chromosomal neighbor *RB1* are frequently codeleted in primary prostate cancer and this codeletion is enriched in mCRPC. Our current study focuses on understanding the molecular consequences of co-loss of *BRCA2 and RB1* in prostate cancer. We observed that CRISPR-mediated knockout of *BRCA2* induces *FOLH1* expression in LNCaP cells. Recently Paschelis and colleagues reported higher membranous *FOLH1*/PSMA expression in patients with mCRPC who harbor deleterious aberration of *BRCA2* [$P < 0.001$; median H-score: 300 (165–300; ref. 56]. Our data indicate that CRISPR-mediated knockout of *BRCA2* LNCaP cells may exhibit molecular features (upregulation of *FOLH1*) similar to those observed in patients with mCRPC who harbor aberration of *BRCA2*. Furthermore, using CRISPR and shRNA-based knockout/knockdown approach, we observed that co-loss of *BRCA2* and *RB1* in LNCaP cells induces an EMT-like invasive phenotype compared with loss of either gene alone. For the first time, we demonstrate that human prostate cancer cells exhibit a distinct phenotype upon co-loss of *BRCA2-RB1* that may lead to aggressive disease.

Biallelic inactivation (germline mutation plus somatic loss of heterozygosity) of *BRCA2* or other DDR genes is often associated with prostate cancer progression. However, the role of heterozygous somatic deletion of *BRCA2* in prostate cancer is poorly understood. In our current study, we show for the first time that heterozygous loss of *BRCA2* significantly reduces BRCA2 protein levels in primary prostate cancer (TCGA cohort). Similarly, in the same cohort, we observed that heterozygous deletion of *RB1* also significantly attenuates *RB1* mRNA expression. Heterozygous deletions are very difficult to analyze by copy number variation algorithms; therefore, we validated the heterozygous deletion of *BRCA2* and *RB1* in mCRPC-derived organoids using FISH. We observed depleted BRCA2 and RB1 protein in the organoids that harbor heterozygous codeletion of a *BRCA2* and *RB1* allele. Our data indicate that heterozygous loss leads to haploinsufficiency of BRCA2 and RB1 protein, which may result in "BRCA2-RB1ness" in prostate cancer. Very recently, Rodrigues and colleagues demonstrated heterogenicity of RB1 expression in advanced mCRPC (57). In the same study, the authors showed that hemizygous/heterozygous loss of one copy of *RB1* in mCRPC was associated with absence of RB1 protein expression, further indicating the presence of haploinsufficiency of RB1 in mCRPC (57). Therefore, heterozygous loss of *BRCA2-RB1* is likely associated with prostate cancer progression even in primary disease. However, this speculation requires further testing in a larger cohort to confirm the prognostic significance of heterozygous loss of *BRCA2* and *RB1* in prostate cancer.

Herein, we showed that PARP inhibition reduces growth of prostate cancer cells that harbor homozygous and, importantly, heterozygous co-loss of *BRCA2* and *RB1*. PARPi have demonstrated promise in treating cancers with DDR deficiencies (20, 58). Our data showed that the castration-resistant prostate cancer cell line LNCaP-Abl and the mCRPC organoids MSK-PCa1 and MSK-PCa3 that harbor heterozygous codeletion of *BRCA2-RB1* (on the basis of 3-color FISH), undergo significant growth inhibition when treated with olaparib or talazoparib. Very recently, Jonsson and colleagues showed that PARPi exhibit significant clinical benefit ($P = 2.2 \times 10^{-5}$) to patients harboring biallelic or even heterozygous loss of *BRCA* (*BRCA1* or *2*) in *BRCA*-associated cancer including prostate cancer (59). Therefore, we hypothesized that patients with mCRPC and potentially high-risk localized disease who are identified as having tumors with codeletion (heterozygous/homozygous) of *BRCA2-RB1* could significantly benefit from PARPi-based therapy.

Recent findings in genetically engineered mice showed that conditional elimination of *BRCA2* in the mouse prostate failed to induce oncogenic transformation (60). *BRCA2* is located on chromosome 13q in close proximity to the RB transcriptional corepressor 1 (*RB1*) gene, and loss of heterozygosity of the *BRCA2* and *RB1* locus is observed in approximately 30% of sporadic breast tumors (61). *RB1* is a gatekeeper gene, whose inactivation is often demonstrated as an important rate-limiting step in tumor initiation (62). We found that *BRCA2* is frequently codeleted with *RB1* and more so in advanced than primary prostate cancer. Codeletion was associated with higher Gleason grade and metastases, while deletion of *RB1* alone was not associated with disease progression. Interestingly, we observed that knockout/knockdown of *RB1* partially attenuates *BRCA2* expression in prostate cancer cells. Furthermore, we also observed that *BRCA2* knockout LNCaP cells exhibit partial loss of *RB1* expression, indicating a possible positive feed-forward loop between *BRCA2* and *RB1* in prostate cancer cells. Previous studies have showed that depletion of *RB1* in osteosarcoma cells displayed spontaneous DNA damage evidence by

Downloaded from http://aacrjournals.org/clincancerres/article-pdf/26/8/2047/2067287/2047.pdf by guest on 27 August 2022

increased γH2AX foci and elevated reactive oxygen species (63) that may lead to loss of *BRCA2* expression. However, multiple molecular mechanisms may be involved in this feed-forward regulation of *BRCA2* and *RB1* and this could be a field of future study. *BRCA2-RB1* codeletion was associated with increased genomic instability, suggesting that such tumors may be particularly aggressive. Although our data do not suggest that *BRCA2-RB1*–null prostate cancer cells are the cell of origin of prostate cancer, detection of this aberration early has importance in that it identifies an aggressive form of the disease.

For over two decades, deletion of chromosome 13q has been known to be a frequent event in prostate cancer (17, 64). Recently, Kluth and colleagues showed that the 13q deletions are heterozygous and associated with high Gleason grade ($P < 0.0001$) and early biochemical recurrence ($P < 0.0001$; ref. 18). We observed an interstitial deletion in the *BRCA2-RB1* region of chromosome 13q evidenced by the loss of mRNA expression of the *BRCA2-RB1* region genes compared with the genes outside this region. Although we were not able to determine the clinical significance of *BRCA2-RB1* interstitial deletion in primary prostate cancer (unpublished observation), we do observe significant attenuation of the mRNA expression of these genes (in the *BRCA2-RB1* region) in mCRPC cases. We showed that coelimination of *BRCA2* and *RB1* is sufficient to induce enzalutamide resistance in human prostate cancer cells. Recently, the antiandrogens enzalutamide, apalutamide, and darolutamide were approved by the FDA for nonmetastatic CRPC (65–67). Identification of the interstitial deletion of the *BRCA2-RB1* region of chromosome 13q may be a biomarker of resistance to antiandrogen therapy.

Previous studies have shown that progression to invasive carcinoma requires loss of epithelial adhesion and polarity and acquisition of an invasive phenotype (68, 69). In some cases, tumor cells hijack a developmental program of gene expression, EMT, to gain invasive capacity (68–70). EMT is often associated with metastasis of various cancer types (70), but the role of EMT in prostate cancer progression is not well characterized. Furthermore, murine models have shown that conditional knockout of *BRCA1* or *BRCA2* is sufficient to induce an EMT-like phenotype in mouse mammary tumors (71, 72). Moreover, EMT is also often associated with CRPC (31, 36). Previous studies found that *BRCA2* germline–mutated prostate cancers are highly invasive (73), and *BRCA2* germline mutations are often associated with *RB1* heterozygous deletion in prostate cancer (19). In transcriptome analysis of *BRCA2-RB1*–deleted cases in TCGA cohort, we identified significant enrichment of the hallmark EMT signature, which is consistent with our experimental observation in *BRCA2-RB1*–null LNCaP cells. To further understand the clinical significance of EMT in prostate cancer, we analyzed the 363 primary prostate cancer samples from the Swedish Watchful Waiting cohort (including 277 indolent and 86 lethal cases; 5-year follow-up) in Oncomine suite (33). We observed that enrichment of the hallmark EMT signature was associated with lethal disease. Our cell line–based observation and analysis in TCGA cohort indicate that codeletion of *BRCA2* and *RB1* may induce an EMT-like phenotype in primary tumors and leads to extravasation of tumor cells and metastatic progression to lethal disease.

We also showed that coelimination of *BRCA2-RB1* induced *SLUG* (SNAI2), SNAIL, and PRRX1 expression. Although knockdown of all 3 genes reduces Matrigel invasion in *BRCA2-RB1*–null prostate cancer cells (**Fig. 3J**), loss of SLUG exhibits a more profound anti-invasive effect compared with loss of SNAIL or PRRX1. Previous studies have shown that SLUG is crucial for TGFβ-induced EMT in prostate cancer and SLUG-positive cells are enriched in advanced prostate cancer (74). Elevated expression of SLUG was also observed in CRPC tissue (46). SLUG had been demonstrated as an androgen-regulated transcription factor that facilitates castration resistance in prostate cancer (46), and here we showed higher SLUG expression in LNCaP-*BRCA2-RB1* cells compared with control cells when exposed to androgen. *BRCA2* negatively regulates SLUG expression and EMT in an experimental model of ovarian cancer, which is also consistent with our current observation (75). Therefore, we suggest SLUG might play an important role in *BRCA2-RB1* loss–mediated EMT transformation of prostate cancer cells and may be a potential driver of aggressive disease. However, considering the complexity of the process, we believe that additional mechanisms may also be involved in dedifferentiation and EMT in *BRCA2-RB1*–null prostate cancer cells, a subject for future investigation.

Previous studies have shown that the fraction of the genome altered is a biomarker associated with prostate cancer progression (76). In our current study, we observed that co-loss of *BRCA2* and *RB1* is associated with a higher fraction of genome altered compared with *RB1* loss alone. Loss of *BRCA1* in a genetically engineered mouse model was sufficient to induce higher fraction of genome altered (77). Earlier studies also showed that *BRCA2*-mutated tumors have high copy number burden (78). Therefore, we postulate that codeletion of *BRCA2* and *RB1* may be an early event associated with, rather than a consequence of, a high fraction of genome altered.

To validate and allow for rapid identification of the codeletion of *BRCA2* and *RB1*, we developed a 3-color FISH-based method. We observed that human prostate cancer cells that harbor single copy deletion of *BRCA2* also exhibit heterozygous deletion of *RB1*. Most importantly, our FISH analysis successfully enabled us to determine the copy number of *BRCA2, RB1*, and chromosome 13q at the single-cell level and enabled us to demonstrate the heterogeneity of prostate cancer. In addition, our FISH data are consistent with the findings in various independent prostate cancer clinical cohorts that *BRCA2* is almost uniformly codeleted (heterozygous) with *RB1*. We extended our FISH analysis to mCRPC-derived organoids and showed that our FISH method was able to detect codeletion of *BRCA2* and *RB1* in organoids, consistent with copy number segment analysis. We also observed that the organoids that harbor the codeletion (MSK-PCa1 and 3) were enzalutamide-resistant, whereas MSK-PCa2, which harbors *RB1* loss alone, exhibits enzalutamide sensitivity (21). The data from the organoids are consistent with our cell line study and further suggest that patients with prostate cancer who harbor *BRCA2-RB1* codeletion in a significant fraction of their primary tumor cells may not benefit from ADT. Our 3-color FISH method is rapid and consistent with genome sequencing data and therefore could be used for early screening of the *BRCA2-RB1* codeletion to identify patients at high risk of this form of aggressive prostate cancer, providing an opportunity for early intervention and targeted treatment.

Disclosure of Potential Conflicts of Interest

P.W. Kantoff is a paid consultant/advisory board member of Bavarian Nordic Immunotherapeutics, SEER Biosciences, DRGT, Progenity, and OncoCellMDX, reports ownership interest (including stocks, patents, etc.) in Context Therapeutics LLC, DRGT, Placon, and SEER Biosciences, and reports other remuneration from/relationships with Merck, Roche, Context Therapeutics LLC, Tarveda Therapeutics, and Adena Health. No potential conflicts of interest were disclosed by the other authors.

Authors' Contributions

Conception and design: G. Chakraborty, P.W. Kantoff
Development of methodology: G. Chakraborty, Y.Z. Mazzu, Y. Chen, G.J. Nanjangud

Downloaded from http://aacrjournals.org/clincancerres/article-pdf/26/8/2047/2067287/2047.pdf by guest on 27 August 2022

Acquisition of data (provided animals, acquired and managed patients, provided facilities, etc.): G. Chakraborty, Y.Z. Mazzu, M.O. Atiq, K. Komura, L. Jehane, R. Hirani, Y. Yoshikawa, G.J. Nanjangud
Analysis and interpretation of data (e.g., statistical analysis, biostatistics, computational analysis): G. Chakraborty, J. Armenia, Y.Z. Mazzu, S. Nandakumar, K. Komura, K. Chadalavada, W. Abida, G.J. Nanjangud, P.W. Kantoff
Writing, review, and/or revision of the manuscript: G. Chakraborty, J. Armenia, Y.Z. Mazzu, S. Nandakumar, K.H. Stopsack, M.O. Atiq, L. Jehane, R. Hirani, Y. Yoshikawa, N.A. Khan, Y. Chen, W. Abida, L.A. Mucci, G.J. Nanjangud, P.W. Kantoff
Administrative, technical, or material support (i.e., reporting or organizing data, constructing databases): G. Chakraborty, S. Nandakumar, G.-S.M. Lee, P.W. Kantoff
Study supervision: G. Chakraborty, G.-S.M. Lee, P.W. Kantoff

Acknowledgments

We thank Ralph Garippa, Qiu Xiang, Hsiu Yu Liu, Yunsi Refermat, and staff of the MSK RNAi Core for CRISPR design and T7 assay, staff of the MSK Integrated Genomics Operation Core for RNA-sequencing services, Cindy Lee of the MSK Human Oncology and Pathogenesis Program for organoid culture, Hui Zhao of cBioPortal for gene ontology submission, Michael McGregor and Amy Plofker (MSK) for editing, and Rileen Sinha (Brigham & Women's Hospital/Broad Institute/Harvard Medical School, Boston, MA) for suggestions. This research is funded, in part, through NIH/NCI Cancer Center Support Grant P30 CA008748 to Memorial Sloan Kettering Cancer Center. G. Chakraborty and K.H. Stopsack were supported by a Prostate Cancer Foundation Young Investigator Award. P.W. Kantoff. and L.A. Mucci were supported by a Prostate Cancer Foundation Challenge Award and by NCI grant 5P01CA228696-02.

The costs of publication of this article were defrayed in part by the payment of page charges. This article must therefore be hereby marked *advertisement* in accordance with 18 U.S.C. Section 1734 solely to indicate this fact.

Received May 30, 2019; revised October 11, 2019; accepted November 27, 2019; published first December 3, 2019.

References

1. Mateo J, Carreira S, Sandhu S, Miranda S, Mossop H, Perez-Lopez R, et al. DNA-repair defects and olaparib in metastatic prostate cancer. N Engl J Med 2015;373:1697–708.
2. Pritchard CC, Mateo J, Walsh MF, De Sarkar N, Abida W, Beltran H, et al. Inherited DNA-repair gene mutations in men with metastatic prostate cancer. N Engl J Med 2016;375:443–53.
3. Robinson D, Van Allen EM, Wu YM, Schultz N, Lonigro RJ, Mosquera JM, et al. Integrative clinical genomics of advanced prostate cancer. Cell 2015;162:454.
4. Jasin M, Haber JE. The democratization of gene editing: insights from site-specific cleavage and double-strand break repair. DNA Repair 2016;44:6–16.
5. Nielsen FC, van Overeem Hansen T, Sorensen CS. Hereditary breast and ovarian cancer: new genes in confined pathways. Nat Rev Cancer 2016;16:599–612.
6. Mandelker D, Zhang L, Kemel Y, Stadler ZK, Joseph V, Zehir A, et al. Mutation detection in patients with advanced cancer by universal sequencing of cancer-related genes in tumor and normal DNA vs. guideline-based germline testing. JAMA 2017;318:825–35.
7. Castro E, Goh C, Leongamornlert D, Saunders E, Tymrakiewicz M, Dadaev T, et al. Effect of BRCA mutations on metastatic relapse and cause-specific survival after radical treatment for localised prostate cancer. Eur Urol 2015;68:186–93.
8. Momozawa Y, Iwasaki Y, Hirata M, Liu X, Kamatani Y, Takahashi A, et al. Germline pathogenic variants in 7,636 Japanese patients with prostate cancer and 12,366 controls. J Natl Cancer Inst 2019Jun 19. [Epub ahead of print].
9. Annala M, Vandekerkhove G, Khalaf D, Taavitsainen S, Beja K, Warner EW, et al. Circulating tumor DNA genomics correlate with resistance to abiraterone and enzalutamide in prostate cancer. Cancer Discov 2018;8:444–57.
10. Thangavel C, Boopathi E, Liu Y, Haber A, Ertel A, Bhardwaj A, et al. RB loss promotes prostate cancer metastasis. Cancer Res 2017;77:982–95.
11. Ku SY, Rosario S, Wang Y, Mu P, Seshadri M, Goodrich ZW, et al. Rb1 and Trp53 cooperate to suppress prostate cancer lineage plasticity, metastasis, and anti-androgen resistance. Science 2017;355:78–83.
12. McNair C, Xu K, Mandigo AC, Benelli M, Leiby B, Rodrigues D, et al. Differential impact of RB status on E2F1 reprogramming in human cancer. J Clin Invest 2018;128:341–58.
13. Sharma A, Yeow WS, Ertel A, Coleman I, Clegg N, Thangavel C, et al. The retinoblastoma tumor suppressor controls androgen signaling and human prostate cancer progression. J Clin Invest 2010;120:4478–92.
14. Abida W, Cyrta J, Heller G, Prandi D, Armenia J, Coleman I, et al. Genomic correlates of clinical outcome in advanced prostate cancer. Proc Natl Acad Sci U S A 2019;116:11428–36.
15. Afonso A, Emmert-Buck MR, Duray PH, Bostwick DG, Linehan WM, Vocke CD. Loss of heterozygosity on chromosome 13 is associated with advanced stage prostate cancer. J Urol 1999;162(3 Pt 1):922–6.
16. Dong JT, Boyd JC, Frierson HF Jr. Loss of heterozygosity at 13q14 and 13q21 in high grade, high stage prostate cancer. Prostate 2001;49:166–71.
17. Hyytinen ER, Frierson HF Jr, Boyd JC, Chung LW, Dong JT. Three distinct regions of allelic loss at 13q14, 13q21-22, and 13q33 in prostate cancer. Genes Chromosomes Cancer 1999;25:108–14.
18. Kluth M, Scherzai S, Buschek F, Fraune C, Moller K, Hoflmayer D, et al. 13q deletion is linked to an adverse phenotype and poor prognosis in prostate cancer. Genes Chromosomes Cancer 2018;57:504–12.
19. Annala M, Struss WJ, Warner EW, Beja K, Vandekerkhove G, Wong A, et al. Treatment outcomes and tumor loss of heterozygosity in germline DNA repair-deficient prostate cancer. Eur Urol 2017;72:34–42.
20. Bhattacharjee S, Nandi S. Synthetic lethality in DNA repair network: a novel avenue in targeted cancer therapy and combination therapeutics. IUBMB Life 2017;69:929–37.
21. Gao D, Vela I, Sboner A, Iaquinta PJ, Karthaus WR, Gopalan A, et al. Organoid cultures derived from patients with advanced prostate cancer. Cell 2014;159:176–87.
22. Komura K, Jeong SH, Hinohara K, Qu F, Wang X, Hiraki M, et al. Resistance to docetaxel in prostate cancer is associated with androgen receptor activation and loss of KDM5D expression. Proc Natl Acad Sci U S A 2016;113:6259–64.
23. Cerami E, Gao J, Dogrusoz U, Gross BE, Sumer SO, Aksoy BA, et al. The cBio cancer genomics portal: an open platform for exploring multidimensional cancer genomics data. Cancer Discov 2012;2:401–4.
24. Gao J, Aksoy BA, Dogrusoz U, Dresdner G, Gross B, Sumer SO, et al. Integrative analysis of complex cancer genomics and clinical profiles using the cBioPortal. Sci Signal 2013;6:pl1.
25. Rhodes DR, Yu J, Shanker K, Deshpande N, Varambally R, Ghosh D, et al. ONCOMINE: a cancer microarray database and integrated data-mining platform. Neoplasia 2004;6:1–6.
26. Armenia J, Wankowicz SAM, Liu D, Gao J, Kundra R, Reznik E, et al. The long tail of oncogenic drivers in prostate cancer. Nat Genet 2018;50:645–51.
27. Baca SC, Prandi D, Lawrence MS, Mosquera JM, Romanel A, Drier Y, et al. Punctuated evolution of prostate cancer genomes. Cell 2013;153:666–77.
28. Barbieri CE, Baca SC, Lawrence MS, Demichelis F, Blattner M, Theurillat JP, et al. Exome sequencing identifies recurrent SPOP, FOXA1 and MED12 mutations in prostate cancer. Nat Genet 2012;44:685–9.
29. Beltran H, Prandi D, Mosquera JM, Benelli M, Puca L, Cyrta J, et al. Divergent clonal evolution of castration-resistant neuroendocrine prostate cancer. Nat Med 2016;22:298–305.
30. Grasso CS, Wu YM, Robinson DR, Cao X, Dhanasekaran SM, Khan AP, et al. The mutational landscape of lethal castration-resistant prostate cancer. Nature 2012;487:239–43.
31. Hieronymus H, Schultz N, Gopalan A, Carver BS, Chang MT, Xiao Y, et al. Copy number alteration burden predicts prostate cancer relapse. Proc Natl Acad Sci U S A 2014;111:11139–44.
32. Kumar A, Coleman I, Morrissey C, Zhang X, True LD, Gulati R, et al. Substantial interindividual and limited intraindividual genomic diversity among tumors from men with metastatic prostate cancer. Nat Med 2016;22:369–78.
33. Setlur SR, Mertz KD, Hoshida Y, Demichelis F, Lupien M, Perner S, et al. Estrogen-dependent signaling in a molecularly distinct subclass of aggressive prostate cancer. J Natl Cancer Inst 2008;100:815–25.

Downloaded from http://aacrjournals.org/clincancerres/article-pdf/26/8/2047/2067287/2047.pdf by guest on 27 August 2022

34. Taylor BS, Schultz N, Hieronymus H, Gopalan A, Xiao Y, Carver BS, et al. Integrative genomic profiling of human prostate cancer. Cancer Cell 2010;18: 11–22.
35. Cancer Genome Atlas Research Network. The molecular taxonomy of primary prostate cancer. Cell 2015;163:1011–25.
36. Zehir A, Benayed R, Shah RH, Syed A, Middha S, Kim HR, et al. Mutational landscape of metastatic cancer revealed from prospective clinical sequencing of 10,000 patients. Nat Med 2017;23:703–13.
37. Chen J, Bardes EE, Aronow BJ, Jegga AG. ToppGene Suite for gene list enrichment analysis and candidate gene prioritization. Nucleic Acids Res 2009;37(Web Server issue):W305–11.
38. Liberzon A, Subramanian A, Pinchback R, Thorvaldsdottir H, Tamayo P, Mesirov JP. Molecular signatures database (MSigDB) 3.0. Bioinformatics 2011;27:1739–40.
39. Liberzon A, Birger C, Thorvaldsdottir H, Ghandi M, Mesirov JP, Tamayo P. The Molecular Signatures Database (MSigDB) hallmark gene set collection. Cell Syst 2015;1:417–25.
40. Gao H, Chakraborty G, Zhang Z, Akalay I, Gadiya M, Gao Y, et al. Multi-organ site metastatic reactivation mediated by non-canonical discoidin domain receptor 1 signaling. Cell 2016;166:47–62.
41. Chakraborty G, Kumar S, Mishra R, Patil TV, Kundu GC. Semaphorin 3A suppresses tumor growth and metastasis in mice melanoma model. PLoS One 2012;7:e33633.
42. Lord CJ, Tutt AN, Ashworth A. Synthetic lethality and cancer therapy: lessons learned from the development of PARP inhibitors. Annu Rev Med 2015;66: 455–70.
43. Barbie DA, Tamayo P, Boehm JS, Kim SY, Moody SE, Dunn IF, et al. Systematic RNA interference reveals that oncogenic KRAS-driven cancers require TBK1. Nature 2009;462:108–12.
44. Chen WS, Alshalalfa M, Zhao SG, Liu Y, Mahal BA, Quigley DA, et al. Novel RB1-loss transcriptomic signature is associated with poor clinical outcomes across cancer types. Clin Cancer Res 2019;25:4290–9.
45. Bello D, Webber MM, Kleinman HK, Wartinger DD, Rhim JS. Androgen responsive adult human prostatic epithelial cell lines immortalized by human papillomavirus 18. Carcinogenesis 1997;18:1215–23.
46. Wu K, Gore C, Yang L, Fazli L, Gleave M, Pong RC, et al. Slug, a unique androgen-regulated transcription factor, coordinates androgen receptor to facilitate castration resistance in prostate cancer. Mol Endocrinol 2012;26: 1496–507.
47. Tapia-Laliena MA, Korzeniewski N, Hohenfellner M, Duensing S. High-risk prostate cancer: a disease of genomic instability. Urol Oncol 2014;32: 1101–7.
48. Barretina J, Caponigro G, Stransky N, Venkatesan K, Margolin AA, Kim S, et al. The Cancer Cell Line Encyclopedia enables predictive modelling of anticancer drug sensitivity. Nature 2012;483:603–7.
49. Qin J, Liu X, Laffin B, Chen X, Choy G, Jeter CR, et al. The PSA(-/lo) prostate cancer cell population harbors self-renewing long-term tumor-propagating cells that resist castration. Cell Stem Cell 2012;10:556–69.
50. Rauh-Adelmann C, Lau KM, Sabeti N, Long JP, Mok SC, Ho SM. Altered expression of BRCA1, BRCA2, and a newly identified BRCA2 exon 12 deletion variant in malignant human ovarian, prostate, and breast cancer cell lines. Mol Carcinog 2000;28:236–46.
51. Drost J, Karthaus WR, Gao D, Driehuis E, Sawyers CL, Chen Y, et al. Organoid culture systems for prostate epithelial and cancer tissue. Nat Protoc 2016;11:347–58.
52. Karthaus WR, Iaquinta PJ, Drost J, Gracanin A, van Boxtel R, Wongvipat J, et al. Identification of multipotent luminal progenitor cells in human prostate organoid cultures. Cell 2014;159:163–75.
53. Wang S, Gao D, Chen Y. The potential of organoids in urological cancer research. Nat Rev Urol 2017;14:401–14.
54. Castro E, Romero-Laorden N, Del Pozo A, Lozano R, Medina A, Puente J, et al. PROREPAIR-B: a prospective cohort study of the impact of germline DNA repair mutations on the outcomes of patients with metastatic castration-resistant prostate cancer. J Clin Oncol 2019;37:490–503.
55. Quigley DA, Dang HX, Zhao SG, Lloyd P, Aggarwal R, Alumkal JJ, et al. Genomic hallmarks and structural variation in metastatic prostate cancer. Cell 2018;174: 758–69.
56. Paschalis A, Sheehan B, Riisnaes R, Rodrigues DN, Gurel B, Bertan C, et al. Prostate-specific membrane antigen heterogeneity and DNA repair defects in prostate cancer. Eur Urol 2019;76:469–78.
57. Nava Rodrigues D, Casiraghi N, Romanel A, Crespo M, Miranda S, Rescigno P, et al. RB1 heterogeneity in advanced metastatic castration-resistant prostate cancer. Clin Cancer Res 2019;25:687–97.
58. D'Andrea AD. Mechanisms of PARP inhibitor sensitivity and resistance. DNA Repair 2018;71:172–6.
59. Jonsson P, Bandlamudi C, Cheng ML, Srinivasan P, Chavan SS, Friedman ND, et al. Tumour lineage shapes BRCA-mediated phenotypes. Nature 2019;571: 576–9.
60. Francis JC, McCarthy A, Thomsen MK, Ashworth A, Swain A. Brca2 and Trp53 deficiency cooperate in the progression of mouse prostate tumourigenesis. PLoS Genet 2010;6:e1000995.
61. Cleton-Jansen AM, Collins N, Lakhani SR, Weissenbach J, Devilee P, Cornelisse CJ, et al. Loss of heterozygosity in sporadic breast tumours at the BRCA2 locus on chromosome 13q12-q13. Br J Cancer 1995;72:1241–4.
62. Di Fiore R, D'Anneo A, Tesoriere G, Vento R. RB1 in cancer: different mechanisms of RB1 inactivation and alterations of pRb pathway in tumorigenesis. J Cell Physiol 2013;228:1676–87.
63. Marshall AE, Roes MV, Passos DT, DeWeerd MC, Chaikovsky AC, Sage J, et al. RB1 deletion in retinoblastoma protein pathway-disrupted cells results in DNA damage and cancer progression. Mol Cell Biol 2019;39:pii: e00105-19.
64. Cooney KA, Wetzel JC, Merajver SD, Macoska JA, Singleton TP, Wojno KJ. Distinct regions of allelic loss on 13q in prostate cancer. Cancer Res 1996;56: 1142–5.
65. Fizazi K, Shore N, Tammela TL, Ulys A, Vjaters E, Polyakov S, et al. Darolutamide in nonmetastatic, castration-resistant prostate cancer. N Engl J Med 2019;380:1235–46.
66. Hussain M, Fizazi K, Saad F, Rathenborg P, Shore N, Ferreira U, et al. Enzalutamide in men with nonmetastatic, castration-resistant prostate cancer. N Engl J Med 2018;378:2465–74.
67. Saad F, Cella D, Basch E, Hadaschik BA, Mainwaring PN, Oudard S, et al. Effect of apalutamide on health-related quality of life in patients with non-metastatic castration-resistant prostate cancer: an analysis of the SPARTAN randomised, placebo-controlled, phase 3 trial. Lancet Oncol 2018;19: 1404–16.
68. Kalluri R, Weinberg RA. The basics of epithelial-mesenchymal transition. J Clin Invest 2009;119:1420–8.
69. Hanahan D, Weinberg RA. Hallmarks of cancer: the next generation. Cell 2011; 144:646–74.
70. Brabletz T, Kalluri R, Nieto MA, Weinberg RA. EMT in cancer. Nat Rev Cancer 2018;18:128–34.
71. Wu ZQ, Li XY, Hu CY, Ford M, Kleer CG, Weiss SJ. Canonical Wnt signaling regulates Slug activity and links epithelial-mesenchymal transition with epigenetic Breast Cancer 1, Early Onset (BRCA1) repression. Proc Natl Acad Sci U S A 2012;109:16654–9.
72. Jaspers JE, Sol W, Kersbergen A, Schlicker A, Guyader C, Xu G, et al. BRCA2-deficient sarcomatoid mammary tumors exhibit multidrug resistance. Cancer Res 2015;75:732–41.
73. Isaacsson Velho P, Silberstein JL, Markowski MC, Luo J, Lotan TL, Isaacs WB, et al. Intraductal/ductal histology and lymphovascular invasion are associated with germline DNA-repair gene mutations in prostate cancer. Prostate 2018;78: 401–7.
74. Liu YN, Abou-Kheir W, Yin JJ, Fang L, Hynes P, Casey O, et al. Critical and reciprocal regulation of KLF4 and SLUG in transforming growth factor beta-initiated prostate cancer epithelial-mesenchymal transition. Mol Cell Biol 2012; 32:941–53.
75. Wang Z, Liu Y, Lu L, Yang L, Yin S, Wang Y, et al. Fibrillin-1, induced by Aurora-A but inhibited by BRCA2, promotes ovarian cancer metastasis. Oncotarget 2015;6:6670–83.
76. Hieronymus H, Murali R, Tin A, Yadav K, Abida W, Moller H, et al. Tumor copy number alteration burden is a pan-cancer prognostic factor associated with recurrence and death. Elife 2018;7:e37294.
77. Liu X, Holstege H, van der Gulden H, Treur-Mulder M, Zevenhoven J, Velds A, et al. Somatic loss of BRCA1 and p53 in mice induces mammary tumors with features of human BRCA1-mutated basal-like breast cancer. Proc Natl Acad Sci U S A 2007;104:12111–6.
78. Castro E, Goh C, Olmos D, Saunders E, Leongamornlert D, Tymrakiewicz M, et al. Germline BRCA mutations are associated with higher risk of nodal involvement, distant metastasis, and poor survival outcomes in prostate cancer. J Clin Oncol 2013;31:1748–57.

Downloaded from http://aacrjournals.org/clincancerres/article-pdf/26/8/2047/2067287/2047.pdf by guest on 27 August 2022